


Anomalous Hall effect in magnetic topological insulators: Semiclassical frameworkAmir Sabzalipour^{1,2} and Bart Partoens¹¹*University of Antwerp, Department of Physics, Groenenborgerlaan 171, 2020 Antwerp, Belgium*²*School of Physics, Institute for Research in Fundamental Sciences (IPM), Tehran 19395-5531, Iran* (Received 6 June 2018; revised manuscript received 22 March 2019; published 15 July 2019)

The anomalous Hall effect (AHE) is studied on the surface of a 3D magnetic topological insulator. By applying a modified semiclassical framework, all three contributions to the AHE, the Berry curvature effect, the side-jump effect and the skew scattering effects are systematically treated, and analytical expressions for the conductivities are obtained in terms of the Fermi level, the spatial orientation of the surface magnetization and the concentration of magnetic and nonmagnetic impurities. We demonstrate that the AHE can change sign by altering the orientation of the surface magnetization, the concentration of the impurities and also the position of the Fermi level, in agreement with recent experimental observations. We show how each contribution to the AHE, or even the whole AHE, can be turned off by properly adjusting the given parameters. For example, one can turn off the anomalous hall conductivity in a system with in-plane magnetization by pushing the system into the fully metallic regime.

DOI: [10.1103/PhysRevB.100.035419](https://doi.org/10.1103/PhysRevB.100.035419)**I. INTRODUCTION**

Topological insulators are a new class of matter that resemble band insulators in the bulk while capable of conducting along gapless states on the surfaces or edges [1–4]. Topological properties of the band structure in these materials protect the metallic surface or edge states, as long as time-reversal or crystalline symmetry is present [5]. Surface states of a 3D topological insulator can be described by an effective 2D massless Dirac Hamiltonian, within a certain energy range [6]. Spin-momentum locking of these massless Dirac fermions prohibits backscattering of the itinerant electrons off nonmagnetic impurities and consequently results in anti-weak localization [7,8]. All these exotic features of topological insulators have attracted a lot of interests theoretically and experimentally [9–11]. Revealing these topological features in surface transport is an important direction of research, and the dependency of the surface charge transport on the type of disorder and the range of disorder-electron interaction has been extensively studied theoretically [12,13].

The collective behavior of randomly distributed pointlike magnetic impurities on the surface and in the bulk of a topological insulator can break time-reversal symmetry and drive the system into a gapped system. This introduced gap in spin space influences, via the spin-orbit coupling, the charge dependent properties of the massive Dirac fermions. As the anomalous Hall effect (AHE) is the manifestation of the Hall effect in systems without time-reversal symmetry, a gaped magnetic topological insulator is a valuable host medium for realizing both the quantized version of the anomalous Hall effect [14–17], and the unquantized version [18,19]. The unquantized version of the AHE as one of the most fundamental transport properties of magnetic materials has been an enigmatic problem for almost a century and still remains a poorly understood phenomenon. Understanding the rich physics behind this effect in different systems presents

a deep insight into magnetic materials, and also enables us to introduce new novel properties which can be used in new devices for prospective technological advances in spintronics, random access memory, etc. [20,21].

Although considerable studies have been devoted to the AHE in different systems and different regimes [22–26], less attention has been paid to this phenomenon in magnetic topological insulators. In this work, we investigate the AHE arising from scatterings of massive Dirac fermions by dilute and randomly placed point-like magnetic and nonmagnetic impurities on the surface of a 3D topological insulator. Based on Boltzmann’s semiclassical framework [27–29] along with a modified relaxation time scheme to capture anisotropic effects [30], we provide a comprehensive analysis of the transport of massive Dirac fermions. Interestingly, our results provide a clear scenario behind the sign change of the AHE via changing the concentration of the impurities or via the value of the gate voltage, as was recently shown experimentally in topological materials [31]. Within the semiclassical regime, we found that the calculated AHE can also change sign if one changes the magnetic easy axis from fully out-of-plane to in-plane. Interestingly, such sign change of the AHE with respect to the spatial orientation of the magnetization has already been experimentally observed in ultrathin $Co^{0.3\text{nm}}/Pd^{0.5\text{nm}}$ multilayers [32]. Besides, it has recently been shown experimentally that the AHE can undergo a sign change by altering the spatial orientation of an applied magnetic field in nonmagnetic $ZrTe_5$, which is a candidate for a Dirac or Weyl semimetal [33]. To the best of our knowledge, a sign change of the AHE with respect to the spatial orientation of the surface magnetization has not been reported experimentally for the surface of a topological insulator, and therefore further experiments on this material can test our model.

In the literature, the AHE that arises from scattering of massive Dirac fermions off nonmagnetic impurities has been studied based on the Boltzmann kinetic equation and the

microscopic Kubo-Streda formalism [34–36], and off magnetic impurities with an out-of plane magnetization based on the kinetic equation for the density matrix [37]. In this work we also stress the importance of the magnetization direction. We thoroughly study the three distinct contributions to the AHE, the contribution arising from the intrinsic Berry-phase curvature [38–40], the extrinsic side-jump effect [41,42], and the skew scattering effect [43]. Fully analytical expressions for these contributions to the anomalous Hall conductivity arising from magnetic impurities with arbitrary magnetization direction are derived. Our method was chosen to properly incorporate this anisotropy of the scattering potential. However, we also apply our method to derive the contributions of nonmagnetic isotropic scatterers. In this way, we complete our discussion and it allows us to compare our results for nonmagnetic impurities with those that already have been reported in literature [34]. Many AHE related experiments have been conducted and in some of them a sign change has been reported against temperature, gate voltage, thickness, etc. Different studies have been performed to understand these observed sign changes [44–47]. One of the main findings of this work is introducing a clear and different scenario behind the sign change in the anomalous Hall conductivity for massive Dirac fermions on the surface of a magnetic TI. Two terms with opposite signs compete simultaneously to take control of this conductivity. These terms consist of contributions from the three different effects which all have a different dependency on the Fermi level, the spatial orientation of the surface magnetization and/or the concentration of impurities. Exerting an external electric field determines the momentum direction of the charge carriers which is locked to their spin. In addition, by altering the orientation of the TI's surface magnetization by an applied field, the strength of the scattering potential can be changed, and by changing the Fermi level, the spin orientation can be altered. Accordingly, size and sign of each contribution can vary. Then, since the relative importance of the total positive and negative terms changes, the AHE can undergo a sign and size change against Fermi level, concentration of impurities and spatial orientation of the surface magnetization. Further, the detailed information of each of the three contributions (intrinsic Berry-phase curvature, side-jump effect and skew scattering effect) to the AHE is hidden in the total value of the experimentally measured AHE. Investigating experimentally each of these contributions to the AHE separately is therefore not possible. To overcome this problem, we indicate the experimental regimes in which each contribution is dominant over the others. We have organized the rest of this paper as follows. In Sec. II, we introduce the effective model of massive Dirac fermions on the surface of a magnetically doped three-dimensional topological insulator. In addition, we present the semiclassical approach to correctly incorporate the side-jump and skew scattering contributions in the AHE dynamics of the charge carriers, and outline the need and use of the generalized relaxation time approach. The obtained results are shown in Sec. III. In Sec. IV, we summarize our findings and conclude with our main results. Finally, some more detailed results are collected in the Appendices, as well as the derivation of important expressions to ease tracing some results presented in the previous sections.

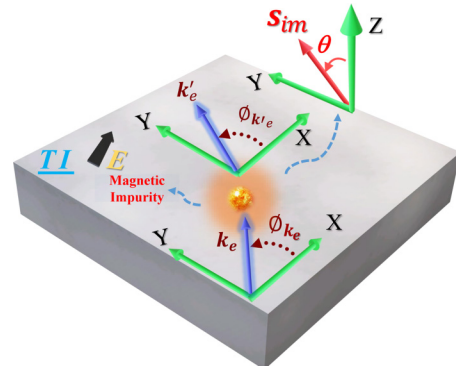


FIG. 1. Schematic overview of the system under study: a magnetic impurity on the surface of a TI, with its magnetization in the yz plane, tilted over an angle θ . An electron with initial wave vector \mathbf{k}_e approaches the impurity and elastically scatters off the impurity with \mathbf{k}'_e as the polar angle for \mathbf{k}'_e .

II. MODEL AND APPROACH

A. Model Hamiltonian

The *minimal* effective Hamiltonian describing massive Dirac fermions on the surface of a 3D TI is given by

$$H_D = \hbar v_F (k \times \sigma)_z + M \sigma_z, \quad (1)$$

where the \hat{z} direction is chosen normal to the surface of the TI. Here, v_F , $\mathbf{k} = (k_x, k_y)$, and M are respectively the Fermi velocity, the wave vector, and the mass of the surface Dirac electrons, and $\sigma = (\sigma_x, \sigma_y, \sigma_z)$ is the vector of Pauli matrices acting on the spin of the electrons. v_F and M are material dependent parameters. For example, in Bi_2Se_3 , $v_F \simeq 5 \times 10^5 \text{ m s}^{-1}$ [48], and Dirac massless fermions have a linear dispersion in the energy range $0 \lesssim E - E_D \lesssim 0.3 \text{ eV}$, with E_D the energy at the Dirac point. In Ref. [49], it was shown that a gap of 50 meV can be introduced in the surface band structure in Fe-doped Bi_2Se_3 , $(\text{Bi}_{0.88}\text{Fe}_{0.12})_2\text{Se}_3$, leading to $M \simeq 25 \text{ meV}$.

The eigenvalues and eigenvectors of H_D are

$$\psi_{k,\alpha}(r) = \frac{e^{i\mathbf{k}\cdot\mathbf{r}}}{\sqrt{A(1 + \xi_k^{2\alpha})}} \begin{pmatrix} e^{-i\phi_k/2} \\ i\alpha \xi_k^\alpha e^{i\phi_k/2} \end{pmatrix}, \quad (2)$$

$$\varepsilon_{k,\alpha} = \alpha \varepsilon_k = \alpha \sqrt{(\hbar v_F k)^2 + M^2}, \quad (3)$$

where α labels the conduction ($\alpha = +1$) and valence ($\alpha = -1$) bands, $k = |\mathbf{k}|$, $\xi_k = \sqrt{(1 - \gamma_k)/(1 + \gamma_k)}$, with $\gamma_k = M/\varepsilon_k$, and $\phi_k = \arctan(k_y/k_x)$ refers to the direction of the wave vector of the surface electrons (see also Fig. 1). In the following, we will also label the eigenstates and energies with the index $l \equiv (k, \alpha)$ as the combined (momentum, band) index.

The presence of dilute and randomly placed magnetic impurities on the surface of a 3D TI, scatter electrons and influence the transport properties of the system. We model the interaction between an electron located at \mathbf{r} and a single magnetic impurity at \mathbf{R}_m as

$$V^m(\mathbf{r} - \mathbf{R}_m) = J \delta(\mathbf{r} - \mathbf{R}_m) \mathbf{S}_m \cdot \mathbf{s}, \quad (4)$$

where \mathbf{S}_m and $\mathbf{s} = \hbar \boldsymbol{\sigma} / 2$ are the spins of the impurity and the electron, respectively. J is the exchange coupling, and

the Dirac delta function refers to the short-range nature of the electron-impurity interaction we have considered in this study. In the regime of large magnetic spin $|S| \rightarrow \infty$, weak interaction $J \rightarrow 0$ and $J|S| = \text{constant}$, we can treat the spin of the magnetic impurities classically. We assume that the magnetic impurities are all aligned in the same direction and lie in the yz plane. Since the system is usually not pure and often also contains nonmagnetic impurities, we also consider, in addition to the term V^m ,

$$V^{nm}(\mathbf{r} - \mathbf{R}_{nm}) = V_0^{nm} \delta(\mathbf{r} - \mathbf{R}_{nm}), \quad (5)$$

as another source for scattering of itinerant electrons off nonmagnetic impurities located at \mathbf{R}_{nm} . The massive Dirac Hamiltonian H_D is a consequence of very strong spin-orbit coupling in the crystal lattice of the TI with many heavy atoms. Therefore, in the presence of such a strong spin-orbit potential, we disregard the correction to Eq. (5) due to the spin-orbit effect of a single impurity atom [43]. We relied on the modified Boltzmann formalism [30] separately for these two kinds of impurities to obtain analytical results for the different contributions to the AHE in a magnetic TI. An overview of the system with some important definitions is shown in Fig. 1.

B. Semiclassical approach

Boltzmann semiclassical approach states

$$-|e|\mathbf{E} \cdot \mathbf{v}_{0l} \left(-\frac{\partial f^0}{\partial \varepsilon_l} \right) = \sum_{l'} w_{ll'} (f_l - f_{l'}), \quad (6)$$

with $\mathbf{v}_{0l} = \frac{1}{\hbar} \nabla_k \varepsilon_k$ the velocity of the incident wave packet, \mathbf{E} is the external applied electric field, $f^0(\varepsilon_l)$ the Fermi-Dirac distribution function, $w_{ll'}$ the transition rate between states l and l' and finally f the distribution function of itinerant electrons. This semiclassical Eq. (6) deals only with gauge invariant quantities, such as the scattering rate, band velocity and the distribution function. Nevertheless, since in this equation the only role of the electric field is to accelerate wave packets, and the only role of impurities is to produce incoherent instantaneous events, it is clear that this approach must often be insufficient. In studying the AHE, more than ever, we need to modify the semiclassical framework to incorporate all the relevant phenomena correctly. We now discuss separately the corrections that are added to the velocity of the electrons, the transition rates and also the distribution function of the electrons in the semiclassical approach, in order to correctly include all phenomena—skew scattering as well as the side-jump and anomalous velocity effects—during the scattering time of electrons off impurities under the presence of an external electric field.

1. Transition rate

To study the transport of electrons in a quantum regime, we need to find the scattering matrix (or T matrix) of the electrons. Within the semiclassical framework, the scattering rate, as a classical object, can be obtained by its connection to the scattering matrix through Fermi's golden rule. However, it should be noted that only the absolute value of the T -matrix elements are present in the scattering rate. Consequently, all

the phase information of the T -matrix elements is lost. In this section, we forget about this insufficiency of the golden rule, but in the following sections we will discuss how we can restore all the missing phase information. The scattering rate between two different quantum states is connected to the T -matrix elements and is given by

$$w_{ll'} = \frac{2\pi}{\hbar} |T_{ll'}|^2 \delta(\varepsilon_{l'} - \varepsilon_l), \quad (7)$$

in which the scattering T matrix is defined as

$$T_{ll'} = \langle l | V_{sc} | \psi_{l'} \rangle, \quad (8)$$

where l is an eigenstate of the Hamiltonian H_D , V_{sc} is the scattering potential operator and $|\psi_{l'}\rangle$ is an eigenstate of the full Hamiltonian $H = H_D + V_{sc}$, that satisfies the Lippmann-Schwinger equation

$$|\psi_{l'}\rangle = |l'\rangle + \frac{V_{sc}}{\varepsilon_{l'} - H_0 + i\eta} |\psi_{l'}\rangle. \quad (9)$$

For weak disorder, $|\psi_{l'}\rangle$ can be approximated by a truncated series in powers of $V_{ll'}$ = $\langle l | V_{sc} | l' \rangle$. By applying Eqs. (9) and (8), $T_{ll'}$ up to third order in V_{sc} is given by

$$T_{ll'} = V_{ll'} + \sum_{l''} \frac{V_{ll''} V_{l''l'}}{\varepsilon_l - \varepsilon_{l''} + i\eta} + \sum_{l'' l'''} \frac{V_{ll''} V_{l''l'''} V_{l'''l'}}{(\varepsilon_l - \varepsilon_{l''} + i\eta)(\varepsilon_l - \varepsilon_{l'''} + i\eta)}. \quad (10)$$

Substituting this expansion for $T_{ll'}$ into Eq. (7) leads to the following scattering rate up to fourth order in the scattering potential:

$$w_{ll'} = w_{ll'}^{(2)} + w_{ll'}^{(3)} + w_{ll'}^{(4)}, \quad (11)$$

where $w_{ll'}^{(2)}$ is symmetric under changing $l \leftrightarrow l'$, and is given by

$$w_{ll'}^{(2)} = \frac{2\pi}{\hbar} \langle |V_{ll'}|^2 \rangle_{\text{dis}} \delta(\varepsilon_l - \varepsilon_{l'}), \quad (12)$$

where “dis” denotes averaging over all possible distributions of impurities in our system. For dilute and randomly placed impurities, it has been shown that $\langle |V_{ll'}|^2 \rangle_{\text{dis}} \sim n_{\text{im}}$ [38], with n_{im} the concentration of impurities. As already indicated, one of the main contributions to the AHE originates from skew scattering. In order to investigate this contribution, we need to calculate the asymmetric part of the transition rate, $w_{ll'}^{(a)} = \frac{w_{ll'} - w_{l'l}}{2}$. Since $w_{ll'}^{(2)}$ is symmetric, the first asymmetric term in the transition rate $w_{ll'}$ appears at the order of V_0^3 . Now $w_{ll'}^{(3)}$ is given by

$$w_{ll'}^{(3)} = \frac{2\pi}{\hbar} \left(\sum_{l''} \frac{\langle V_{ll''} V_{l''l'} V_{l'l} \rangle_{\text{dis}}}{\varepsilon_l - \varepsilon_{l''} - i\eta} + \text{c.c.} \right) \delta(\varepsilon_l - \varepsilon_{l'}). \quad (13)$$

$w_{ll'}^{(3)}$ itself can be written as a sum of a symmetric term $w_{ll'}^{(3s)}$ and an asymmetric term $w_{ll'}^{(3a)}$. Then, $w_{ll'}^{(3)} = w_{ll'}^{(3a)} + w_{ll'}^{(3s)}$, where $w_{ll'}^{(3s/a)} = \frac{w_{ll'}^{(3)} \pm w_{l'l}^{(3)}}{2}$. Since the symmetric part of $w_{ll'}^{(3)}$

$$w_{ll'}^{(3s)} = \frac{4\pi}{\hbar} P \left(\sum_{l''} \frac{\text{Re}[\langle V_{ll''} V_{l''l'} V_{l'l} \rangle_{\text{dis}}]}{\varepsilon_l - \varepsilon_{l''}} \right), \quad (14)$$

just renormalizes $w_{ll'}^{(2)}$, it does not introduce a new physical contribution to the scattering and is further not considered. Note, P in the above equation refers to the *principal value*. The remaining asymmetric term $w_{ll'}^{(3a)}$ can be expressed as

$$w_{ll'}^{(3a)} = \frac{-(2\pi)^2}{\hbar} \delta(\varepsilon_l - \varepsilon_{l'}) \sum_{l''} \text{Im} \langle (V_{ll'} V_{l'l''} V_{l''l})_{\text{dis}} \rangle \delta(\varepsilon_l - \varepsilon_{l''}). \quad (15)$$

This contribution scales with the impurity concentration (for a so-called non-Gaussian disorder model [38]) as $\langle (V_{ll'} V_{l'l''} V_{l''l})_{\text{dis}} \rangle \sim n_{\text{im}}$. Consequently we can expect that the transverse conductivity associated to this term will be inversely proportional to n_{im} [38]. Therefore this contribution to the conductivity of the system dominates in very dilute systems.

Two different scattering processes contribute to the fourth-order expression for the scattering rate. A fourth-order scattering process can occur at a single defect, but also two second-order scattering processes can occur at two different defects. As the sequence of scatterings that lead to these two second-order pair scattering events is arbitrary, this process leads to three contributions in the expression for $w_{ll'}^{(4)}$ [50]:

$$\begin{aligned} w_{ll'}^{(4)} = & \left(\sum_{l''} \sum_{l'''} \left[\frac{\langle V_{l''l} V_{ll''} \rangle_{\text{dis}}}{\varepsilon_l - \varepsilon_{l''} + i\eta} \frac{\langle V_{l''l'''} V_{l''l''} \rangle_{\text{dis}}}{\varepsilon_{l''} - \varepsilon_{l'''} - i\eta} \right] \right. \\ & + \sum_{l''} \sum_{l'''} \left[\frac{\langle V_{l''l} V_{ll''} \rangle_{\text{dis}}}{\varepsilon_l - \varepsilon_{l''} - i\eta} \frac{\langle V_{l''l'''} V_{l''l''} \rangle_{\text{dis}}}{\varepsilon_{l''} - \varepsilon_{l'''} - i\eta} + \text{c.c.} \right] \\ & \left. + \sum_{l''} \sum_{l'''} \left[\frac{\langle V_{ll''} V_{l''l'''} \rangle_{\text{dis}}}{\varepsilon_l - \varepsilon_{l''} - i\eta} \frac{\langle V_{l''l'''} V_{l''l} \rangle_{\text{dis}}}{\varepsilon_{l''} - \varepsilon_{l'''} - i\eta} + \text{c.c.} \right] \right) \\ & \times \delta(\varepsilon_k - \varepsilon_{k'}). \end{aligned} \quad (16)$$

The factors like $\langle V_{l''l} V_{ll''} \rangle_{\text{dis}}$ are all proportional to n_{im} , and therefore these contributions to $w_{ll'}^{(4)}$ are proportional to n_{im}^2 . The fourth-order contribution due to a scattering event at a single impurity contains factors like $\langle V_{ll''} V_{l''l'''} V_{l''l''} V_{l''l} \rangle_{\text{dis}}$ which are proportional to n_{im} . This non-Gaussian correlation yields a term in the transition rate which is physically similar to $w_{ll'}^{(3a)}$ (with respect to the concentration of impurities) but much smaller. Therefore we only consider the contribution of the two second-order pair scattering events in $w_{ll'}^{(4)}$. The term $w_{ll'}^{(4)}$ expressed above is responsible for producing the second contribution of the skew scattering in the anomalous Hall conductivity, in the noncrossing approximation, similar to the results presented in the Appendix of Ref. [50]. This second contribution of the skew scattering is disorder-independent, as will be shown later. In this work, we are interested in the zero temperature regime. Furthermore, in the weak disorder limit that we consider, the energy width of the Bloch state spectral peaks is smaller than the gap, allowing us to ignore direct interband scattering. Therefore we will only consider intraband transitions in calculating $w_{ll'}^{(2)}$ and $w_{ll'}^{(3)}$. We consider electron transport in electron doped systems, thus the Fermi level ε_F lies inside the conduction band, consequently $\alpha = +1$ for all states in Eqs. (12) and (15). However, for $w_{ll'}^{(4)}$, we also incorporate the off-diagonal scattering matrix elements as they produce virtual transitions that mix states in the two

bands in a way which is ultimately crucial [34]. Thus for the calculation of $w_{ll'}^{(4)}$, also interband virtual transitions with $\alpha, \alpha' = \pm 1$ are taken into account.

2. Electron velocity

To obtain the current density of the system $\mathbf{J} = \sum_l \mathbf{v}_l f_l$, we need to calculate the velocity \mathbf{v}_l of the itinerant electrons and also their distribution function f_l in the presence of an external electric field and randomly placed dilute magnetic and nonmagnetic impurities. The conventional semiclassical approach just studies electrons at scattering events and ignores the evolution of the wave packets during the scattering time interval where a side jump can occur. Furthermore, in a system with broken either time-reversal or inversion symmetries, an additional term should be added to the velocity expression of electrons to incorporate properly the effect of the nonzero Berry-phase curvature in the electron dynamics. If we incorporate both extra effects, which are missing in the conventional semiclassical approach, the velocity can be written as

$$\mathbf{v}_l = \mathbf{v}_{0l} + \mathbf{v}_l^{\text{an}} + \mathbf{v}_l^{\text{sj}}, \quad (17)$$

in which $\mathbf{v}_l^{\text{an}} = -\dot{\mathbf{k}} \times (\nabla_{\mathbf{k}} \times \mathbf{A}_l)$ is the anomalous velocity, with $\mathbf{A}_l = i \langle u_l | \nabla_{\mathbf{k}} | u_l \rangle$ the Berry connection where $u_l(\mathbf{r}) = e^{-i\mathbf{k} \cdot \mathbf{r}} \psi_l(\mathbf{r})$, and $\mathbf{v}_l^{\text{sj}} = \sum_{l''} \delta \mathbf{r}_{ll''} w_{ll''}$ is the side-jump velocity. Here, $\delta \mathbf{r}_{ll''}$ denotes the anomalous deflection which electrons experience during scattering time. The gauge invariant expression of this anomalous displacement is given by [28]

$$\delta \mathbf{r}_{ll''} = \mathbf{A}_{l''} - \mathbf{A}_l - (\nabla_{\mathbf{k}} + \nabla_{\mathbf{k}}) \arg(V_{ll''}), \quad (18)$$

where $\arg(V_{ll''})$ is the argument of $V_{ll''}$. While the phase information of the scattering amplitude is absent in the first-order Born approximation, the third term on the right hand side of Eq. (18) is responsible for restoring this information to the dynamics of the charge carriers.

3. Distribution function

After obtaining all terms for the velocity expression of the electrons, the next step is to calculate the distribution function of the electrons. Therefore we write the electron distribution function as follows:

$$f_l = f^0 + g_l^s + g_l^{a1} + g_l^{a2} + g_l^{ad}. \quad (19)$$

The largest deviation from the Fermi-Dirac distribution is given by g_l^s . It arises from the symmetric part of the scattering rate $w_{ll'}^{(2)}$ and also describes the longitudinal conductivity. g_l^{a1} is defined as the deviation due to the asymmetric part of the scattering rate $w_{ll'}^{(3a)}$, and g_l^{a2} due to $w_{ll'}^{(4)}$. Finally, g_l^{ad} is responsible for capturing the effect of the side jump which changes the energy of the scattered electrons and consequently their distribution function. Substituting the transition rate $w_{ll'}$ expressed in Eq. (11) along with the above nonequilibrium distribution function into Eq. (6), we obtain the following self-consistent time-independent integral equations:

$$-e\mathbf{E} \cdot \mathbf{v}_{0l} \left(-\frac{\partial f^0}{\partial \varepsilon_l} \right) = \sum_{l'} w_{ll'}^{(2)} (g_l^s - g_{l'}^s), \quad (20)$$

$$\sum_{l'} w_{ll'}^{(3a)} (g_l^s - g_{l'}^s) + \sum_{l'} w_{ll'} (g_l^{a1} - g_{l'}^{a1}) = 0, \quad (21)$$

$$-e\mathbf{E} \cdot \mathbf{v}_l^{sj} \left(-\frac{\partial f^0}{\partial \varepsilon_l} \right) = \sum_{l'} w_{ll'} (g_l^{ad} - g_{l'}^{ad}), \quad (22)$$

$$\sum_{l'} w_{ll'}^{(4)} (g_l^s - g_{l'}^s) + \sum_{l'} w_{ll'} (g_l^{a2} - g_{l'}^{a2}) = 0. \quad (23)$$

In the presence of an external electric field \mathbf{E} , electrons acquire an extra potential energy $\Delta U_{ll'} = -e\mathbf{E} \cdot \delta\mathbf{r}_{ll'}$ during the side jump $\delta\mathbf{r}_{ll'}$. Since the energy of the electrons is conserved during elastic scattering, this change in potential energy during a side-jump event should be compensated by a change in the kinetic energy of the electrons given by $\Delta\varepsilon_{ll'} = \varepsilon_{l'} - \varepsilon_l = e\mathbf{E} \cdot \delta\mathbf{r}_{ll'}$. Therefore, based on conservation of energy, one obtains $\sum_{l'} w_{ll'} [(f^0(\varepsilon_l) - f^0(\varepsilon_{l'}))] = -e\mathbf{E} \cdot \mathbf{v}_l^{sj} \left(-\frac{\partial f^0}{\partial \varepsilon_l} \right)$, which reduces to Eq. (22) based on $\sum_{l'} w_{ll'} [(f^0(\varepsilon_l) + g_l^{ad}) - (f^0(\varepsilon_{l'}) + g_{l'}^{ad})] = 0$. As g_l^{a1} , g_l^{a2} and g_l^{ad} are small compared to g_l^s , we approximate $w_{ll'}$ in Eqs. (21)–(23) by $w_{ll'}^{(2)}$.

It is now interesting to deduce how each contribution to the distribution function scales with the impurity concentration. Since $w_{ll'}^{(2)} \sim n_{\text{im}}$, we find, based on equation Eq. (20), that $g_l^s \sim n_{\text{im}}^{-1}$. Like $w_{ll'}^{(2)}$, $w_{ll'}^{(3a)} \sim n_{\text{im}}$, therefore referring to Eq. (21) shows that $g_l^{a1} \sim n_{\text{im}}^{-1}$. As it is clear that $\mathbf{v}_l^{sj} \sim w_{ll'}^{(2)} \sim n_{\text{im}}$, then based on Eq. (22), one can conclude that $g_l^{ad} \sim n_{\text{im}}^0$. Finally, let us consider g_l^{a2} . Since $w_{ll'}^{(4)} \sim n_{\text{im}}^2$ and $g_l^s \sim n_{\text{im}}^{-1}$ we come to the conclusion that $g_l^{a2} \sim n_{\text{im}}^0$.

4. Current density

The next step is to calculate the relevant terms in the current density. Using Eqs. (17) and (19), the charge current density is given by

$$\begin{aligned} \mathbf{J} &= -e \sum_l f_l \mathbf{v}_l \\ &\simeq \mathbf{J}^{\text{an}} + \mathbf{J}^s + \mathbf{J}^{ad} + \mathbf{J}^{sj} + \mathbf{J}^{sk1} + \mathbf{J}^{sk2}, \end{aligned} \quad (24)$$

where $\mathbf{J}^{\text{an}} = -e \sum_l f_l^0(\varepsilon_l) \mathbf{v}_l^{\text{an}}$ is the anomalous current density, $\mathbf{J}^s = -e \sum_l g_l^s \mathbf{v}_{0l}$ is the regular contribution to the charge current, arising from impurity scattering events within the first-order Born approximation, $\mathbf{J}^{ad} = -e \sum_l g_l^{ad} \mathbf{v}_{0l}$ and $\mathbf{J}^{sj} = -e \sum_l g_l^s \mathbf{v}_l^{sj}$ are consequences of the side-jump effect on the distribution function and the electron velocity, respectively. $\mathbf{J}^{sk1} = -e \sum_l g_l^{a1} \mathbf{v}_{0l}$ and $\mathbf{J}^{sk2} = -e \sum_l g_l^{a2} \mathbf{v}_{0l}$ result from skew scattering. In the second line of Eq. (24), among the 15 terms we just consider 6 terms nonnegligible. It is obvious that $\sum_l f_l^0(\mathbf{v}_{0l} + \mathbf{v}_l^{sj}) = 0$ for the equilibrium distribution function. In addition, we have ignored the small contributions $\sum_l (g_l^{a1} + g_l^{a2} + g_l^{ad}) \mathbf{v}_l^{sj}$. Moreover, as \mathbf{v}_{an} is already linear in the electric field, the nonlinear contributions to the current $\sum_l (g_l^s + g_l^{a1} + g_l^{a2} + g_l^{ad}) \mathbf{v}_l^{\text{an}}$ are also omitted.

C. Generalized relaxation time approximation

In order to solve the integral equations (20)–(23), we rely on the generalized relaxation-time approach introduced first in Ref. [30]. When both the energy spectrum and the scattering potential are isotropic, the transition probability $w_{ll'}$ will depend only on the angle between k and k' , and one can employ the standard relaxation time approach [51]. This is

indeed the case when the spins of the magnetic impurities in Eq. (4) are aligned perpendicular to the surface, i.e., $\mathbf{S}_m = S_m \hat{z}$. On the other hand, for an arbitrary orientation of the spins of the aligned magnetic impurities, the scattering of helical electrons becomes anisotropic and the transition probability depends on the directions of both k and k' . Consequently, the relaxation time is strongly anisotropic and depends on the magnitude and direction of k , and on the orientation of the magnetic impurities. The generalized relaxation time approximation captures the effects of this anisotropy in the conductivity [30]. In this approach, the different contributions to the nonequilibrium distribution function are written as

$$g_l^p = eE [\lambda_{1l}^p \cos \chi + \lambda_{2l}^p \sin \chi] \frac{\partial f^0}{\partial \varepsilon_l}. \quad (25)$$

Here, p stands for s , $a1$, $a2$, and ad . χ is the angle of \mathbf{E} with the \hat{x} direction, λ_{il}^p ($i = 1, 2$) are the generalized mean free paths of the charge carriers. In anisotropic systems, the size of the mean free paths of electrons depends on the relative direction of the drift velocity of the electrons respect to the external electric field. Hence, in order to capture this anisotropy, two different mean free paths are introduced in the proposal for the electron distribution function, namely λ_{1l}^p and λ_{2l}^p . λ_{1l}^p corresponds to those electrons that move parallel to the external electric field and λ_{2l}^p for those electrons that move perpendicular to the external electric field. Then, since in isotropic systems, electrons feel the same scattering potential in every direction, the form of this proposal for the distribution function of the electrons reduces to the well-known relaxation time formalism in isotropic systems.

Considering now an electric field in the \hat{x} or \hat{y} direction $\mathbf{E} = E \hat{x}_i$ ($\hat{x}_1 = \hat{x}$, $\hat{x}_2 = \hat{y}$) and substituting g_l^p from Eq. (25) into Eqs. (20)–(23), we arrive at

$$\mathbf{v}_{0l} \cdot \hat{x}_i = \sum_{l'} w_{ll'}^{(2)} [\lambda_{il}^s - \lambda_{il'}^s], \quad (26)$$

$$\mathbf{v}_l^{sj} \cdot \hat{x}_i = \sum_{l'} w_{ll'}^{(2)} [\lambda_{il}^{ad} - \lambda_{il'}^{ad}], \quad (27)$$

$$\sum_{l'} w_{ll'}^{(2)} [\lambda_{il}^{a1} - \lambda_{il'}^{a1}] + \sum_{l'} w_{ll'}^{(3a)} [\lambda_{il}^s - \lambda_{il'}^s] = 0, \quad (28)$$

$$\sum_{l'} w_{ll'}^{(4)} [\lambda_{il}^s - \lambda_{il'}^s] + \sum_{l'} w_{ll'}^{(2)} [\lambda_{il}^{a2} - \lambda_{il'}^{a2}] = 0. \quad (29)$$

To solve the above equations, all mean free paths λ_{il}^p are expanded in Fourier series. Finally we obtain the Fourier coefficients of $\lambda_i^{m,p}$, the general mean free path of the Dirac fermions due to scattering off magnetic impurities, and also the Fourier coefficients of $\lambda_i^{nm,p}$, the general mean free path of the Dirac fermions due to scattering off nonmagnetic impurities.

III. RESULTS AND DISCUSSIONS

In this section, we present our results for the anomalous Hall response on the surface of a 3D topological insulator. Different regimes can be identified. As shown in the previous section, some contributions to the anomalous Hall conductivity are independent of the impurity concentration, others are inversely proportional. Therefore we can express

the anomalous Hall conductivity of the system as

$$\sigma_{ij}^{\text{AHE}} = \sigma_{ij}^{\text{int. AHE}} + \sigma_{ij}^{\text{ext. AHE}}, \quad (30)$$

where we label the term $\sigma_{ij}^{\text{ext. AHE}}$ as extrinsic because it depends on the concentration of impurities, while we label the term $\sigma_{ij}^{\text{int. AHE}}$ as intrinsic because it is independent of the concentration of impurities. If only the first term is significant and the second term is negligible, we call this regime the intrinsic regime, and when the first term is very small and negligible the system is in the extrinsic regime. If both contributions are comparable, the systems is in the intermediate regime. Since the anomalous Hall response of the system behaves differently in these distinctive regimes, they are discussed separately in the following sections.

A. The intrinsic regime

$\sigma_{ij}^{\text{int. AHE}}$ originates from three effects simultaneously, namely the Berry-phase curvature, the side-jump effect and the skew scattering. Except the contribution arising from the Berry-phase curvature, the other contributions in this regime originate from the impurities, even though the expressions of their corresponding conductivities do not depend on the concentration of impurities. To better understand the behavior of $\sigma_{ij}^{\text{int. AHE}}$, each of these contributions is discussed separately in Secs. III A 1–III A 3. Finally, after discussing comprehensively these involved contributions, the anomalous Hall conductivity in the intrinsic regime is studied in Sec. III A 4.

1. Berry curvature contribution

Unlike side jump and skew scattering, this contribution does not rely on the presence of impurities and interestingly produces a nonzero conductivity even in a pure system. As we already mentioned, the nonzero Berry-phase curvature causes an anomalous velocity \mathbf{v}_i^{an} and consequently contributes to the AHE by $\mathbf{J}^{\text{an}} = -e \sum_l f^0(\varepsilon_l) \mathbf{v}_l^{\text{an}}$. In order to calculate this term, one has to consider the contributions of all electrons residing in the whole Fermi sea, instead of just considering those electrons in the conduction band. Using the eigenstates in Eq. (2), one arrives at the following expression for the

anomalous velocity:

$$\mathbf{v}_{k,\alpha}^{\text{an}} = -\hat{\mathbf{k}} \times \Omega_{k,\alpha} = \frac{e\mathbf{E}}{\hbar} \times \frac{-\alpha M v_F^2 \hbar^2}{2(k^2 v_F^2 \hbar^2 + M^2)^{3/2}} \hat{\mathbf{z}}. \quad (31)$$

This correction to the velocity of electrons produces following contribution to the conductivity of the system:

$$\sigma_{xy}^{\text{an}} = -e \left(\sum_{k=0}^{k_F} \mathbf{v}_{k,+}^{\text{an}} / E_y + \sum_{k=0}^{\infty} \mathbf{v}_{k,-}^{\text{an}} / E_y \right) = -\frac{1}{2m}, \quad (32)$$

with $\sigma_{yx}^{\text{an}} = -\sigma_{xy}^{\text{an}}$ and $m = \frac{\varepsilon_F}{M}$. Note that all contributions to the AHE, like the expression above, are given in units of $\frac{e^2}{h}$. This contribution can be regarded as an “unquantized” version of the quantum Hall effect which is given by $\sigma_{xy}^{\text{QHE}} = -\frac{1}{2}$. This term changes within $0 \leq |\sigma_{ij}^{\text{an}}[m]| \leq 0.5$, if $1 \leq m \leq \infty$ and since is inversely proportional to $m = \frac{\varepsilon_F}{M}$, it obviously turns off in the gapless regime ($M = 0$). We will show that of the three involved contributions to the AHE, this contribution dominates the AHE when $m = 1$, not only in the intrinsic regime but also in the intermediate regime.

2. Side-jump related contributions

As we indicated before, there are two distinct effects due to the anomalous coordinate shift: the side jump $\delta \mathbf{r}_{kk'}$ and a change in the energy of the electron. After averaging over many scattering events, side jumps do not cancel out and give rise to a nonzero contribution $\mathbf{v}_{k'}^{sj}$ to the velocity of the electrons given in Eq. (17). This correction to the velocity of the electrons itself changes the conductivity of the electrons and we call this contribution σ_{ij}^{sj} . The second effect is the energy change of an electron when it makes a deflection $\delta \mathbf{r}_{kk'}$ in the presence of an external electric field \mathbf{E} . This change in its potential energy is given by $e \delta \mathbf{r}_{kk'} \cdot \mathbf{E}$, which eventually leads to the deviation of the distribution function of the electrons that we indicate as g_l^{ad} in Eq. (19). We now separately discuss the resultant conductivities σ_{ij}^{sj} and σ_{ij}^{ad} .

Using the eigenvectors of the conductive massive Dirac fermions given in Eq. (2) and applying Eq. (18), we obtain the deflections $\delta \mathbf{r}_{kk'}^m$ and $\delta \mathbf{r}_{kk'}^{nm}$ due to the scattering off magnetic and nonmagnetic impurities, and they are given by

$$\delta \mathbf{r}_{kk'}^m \left[\frac{\hbar v_F}{\varepsilon_k} \right] = \frac{\gamma(1/2 - c)}{\sqrt{(1 - \gamma^2)}} [\hat{\phi}_{k'} - \hat{\phi}_k] + c \tan \theta [\cos \phi_{k'} \hat{\phi}_k - \cos \phi_k \hat{\phi}_{k'}] + (2c\gamma^2 \tan \theta \sin \phi_- \cos \phi_+ - c\sqrt{\gamma^2 - \gamma^4} \sin 2\phi_-) [\hat{\mathbf{k}} + \hat{\mathbf{k}}'], \quad (33)$$

$$\delta \mathbf{r}_{kk'}^{nm} \left[\frac{\hbar v_F}{\varepsilon_k} \right] = \frac{\gamma(1 - \gamma^2)^{1/2}}{4(\cos^2 \phi_- + \gamma^2 \sin^2 \phi_-)} (\sin 2\phi_- [\hat{\mathbf{k}} + \hat{\mathbf{k}}'] - 2 \sin^2 \phi_- [\hat{\phi}_{k'} - \hat{\phi}_k]), \quad (34)$$

where the two vectors $\hat{\mathbf{k}}$ and $\hat{\phi}_k$ are unit vectors in spherical coordinates, respectively in the radial and polar direction, θ is the tilting angle of the randomly placed point-like magnetic impurities on the surface of the magnetic TI, $\gamma = \gamma_k = \frac{M}{\varepsilon_k}$, $\phi_{\pm} = \frac{\phi_k \pm \phi_{k'}}{2}$, and finally $c = (2 \sin^2 \phi_- + 2[\gamma_k \cos \phi_- + \sqrt{1 - \gamma_k^2} \tan \theta \cos \phi_+]^2)^{-1}$. Since

electrons undergo two distinctive and independent scattering events, magnetic and nonmagnetic, we treat them separately. As Eq. (33) shows, the side jump of an electron during a magnetic scattering strongly depends on its incident angle ϕ_k , scattering angle $\phi_{k'}$ and also θ , the tilting angle with respect to the $\hat{\mathbf{z}}$ direction of the magnetic orientation of the surface impurities.

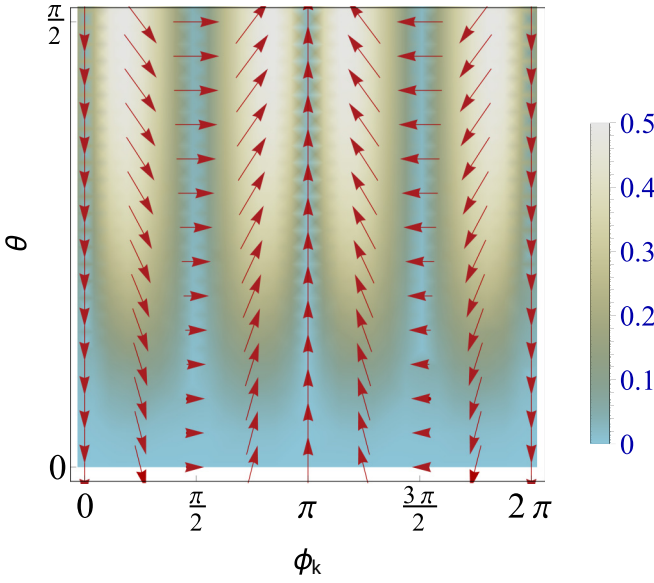


FIG. 2. $\mathbf{v}_k^{m.sj}$ is shown as a function of ϕ_k and θ , with $\vartheta_k^m = 1$. The background color shows $\cos \varphi$, with φ the angle between $\mathbf{v}_k^{m.sj}$ and \mathbf{v}_{0k} .

Using the derived side jumps $\delta \mathbf{r}_{kk'}$ for magnetic and nonmagnetic scattering events, we can obtain the following side-jump velocities:

$$\mathbf{v}_k^{m.sj} = \vartheta_k^m [(1 + 2 \sin^2 \theta) \sin \phi_k \hat{x} - \cos \phi_k \hat{y}], \quad (35)$$

$$\mathbf{v}_k^{nm.sj} = \vartheta_k^{nm} \hat{\phi}_k, \quad (36)$$

where $\vartheta_k^m = \frac{S_m^2 J^2 n_{\text{im}}}{8 \hbar^2 v_F} \Lambda_k$ and $\vartheta_k^{nm} = \frac{V_G^2 n_{\text{im}}}{2 \hbar^2 v_F} \Lambda_k$ with $\Lambda_k = \gamma_k \sqrt{1 - \gamma_k^2}$ and n_{im} the concentration of the nonmagnetic impurities. Both of these velocity expressions are only nonzero for gaped systems (i.e., $\gamma_k \neq 0$) and therefore this effect is a consequence of the gap opening. Also note that Eqs. (35) and (36) show that $\mathbf{v}_k^{m.sj}$ is always perpendicular to the band velocity \mathbf{v}_{0k} (directed in the $\hat{\mathbf{k}}$ direction), in contrary to $\mathbf{v}_k^{m.sj}$. Only when all magnetic impurities are aligned perpendicular to the surface of the TI (i.e., $\theta = 0$) or when the electrons move on the surface of the TI in the direction perpendicular to the in-plane component of the magnetization (i.e., $\phi_k = 0$) we find $\mathbf{v}_k^{m.sj} \parallel \mathbf{v}_k^{nm.sj}$.

To better trace the behavior of the side-jump velocity of the electrons during a magnetic scattering event, Fig. 2 is provided to show $\mathbf{v}_k^{m.sj}$ as function of θ and ϕ_k . Here, ϑ_k^m was set to 1 and the background color shows $\cos \varphi$, with φ the angle between $\mathbf{v}_k^{m.sj}$ and \mathbf{v}_{0k} . This figure now reveals when the side-jump contribution to the transverse conductivity is largest. As it is shown, by increasing θ the side-jump velocity $\mathbf{v}_k^{m.sj}$ increases (indicated by the increase in length of the red arrows in Fig. 2), most clear around $\phi_k = \pi/2$ and $3\pi/2$, and consequently a larger transverse conductivity can be expected. The averaged band velocity of itinerant electrons in the presence of an external electric field along the \hat{x}/\hat{y} direction would be along the $-\hat{x}/-\hat{y}$ direction, corresponding to $\phi_k = \pi$ and $\frac{3\pi}{2}$, respectively. This figure shows that the side-jump velocity $\mathbf{v}_k^{m.sj}$ of electrons for $\phi_k = \pi$ is along

the \hat{y} direction and for $\phi_k = \frac{3\pi}{2}$ is along the $-\hat{x}$ direction. Therefore we can expect that $\sigma_{yx}^{m.sj} < 0$ and $\sigma_{xy}^{m.sj} > 0$ for the corresponding transverse conductivities. Furthermore, from the background color of Fig. 2 which shows $\cos \varphi$ with φ the angle between $\mathbf{v}_k^{m.sj}$ and \mathbf{v}_{0k} , we can deduce that the area for which $\mathbf{v}_k^{m.sj} \cdot \mathbf{v}_{0k} \sim 0$ is larger around $\phi_k = \frac{3\pi}{2}$ than for $\phi_k = \pi$. Therefore we expect $|\sigma_{xy}^{m.sj}| > |\sigma_{yx}^{m.sj}|$. Now we are ready to derive all side-jump contributions in the charge current of the massive Dirac fermions due to the magnetic impurities $\mathbf{J}^{\text{tot}.m.sj} = \mathbf{J}^{m.sj} + \mathbf{J}^{m.ad}$ and the nonmagnetic impurities $\mathbf{J}^{\text{tot}.nm.sj} = \mathbf{J}^{nm.sj} + \mathbf{J}^{nm.ad}$. In order to find $\mathbf{J}^{m.ad}$ and $\mathbf{J}^{nm.ad}$, we need to solve the corresponding Eq. (27). We obtain all the mean free paths $\lambda_i^{m.ad}$ and $\lambda_i^{nm.ad}$ by relying on their Fourier expansions (the expressions are given in Appendix B) and obtain the following corresponding charge conductivities

$$\sigma_{xy}^{m.ad} = \frac{2(1 - m^2)}{4m(4m^2 \cos^2 \theta + g(m^2 + \cos 2\theta))}, \quad (37)$$

$$\sigma_{yx}^{m.ad} = \frac{(2 - \cos 2\theta)(m^2 + \cos 2\theta)(g - 2)}{4m(\cos 4\theta - 1 + (m^2 + \cos 2\theta)(g - 2))}, \quad (38)$$

$$\sigma_{xy}^{nm.ad} = -\sigma_{yx}^{nm.sj} = \frac{1 - m^2}{m(m^2 + 3)}, \quad (39)$$

with $g = \frac{(4(m^4+1)+2m^2(4 \cos 2\theta + \cos 4\theta - 1))^{1/2}}{|m^2 + \cos 2\theta|}$. Because $\mathbf{J}^{sj} = -e \sum_{\mathbf{k}} g_{\mathbf{k}}^s \mathbf{v}_{\mathbf{k}}^{sj}$ and using the already reported distribution function $g_{\mathbf{k}}^s$ in Ref. [52], we come to the conclusion that $\sigma_{ij}^{m.sj} = \sigma_{ji}^{m.ad}$ and $\sigma_{ij}^{nm.sj} = \sigma_{ij}^{nm.ad}$, for $i \neq j$. Equation (39) for nonmagnetic impurities agrees with the result reported in Ref. [34]. However, in contrary to Ref. [34], which indicates that in general $\sigma_{ij}^{sj} = \sigma_{ij}^{ad}$ for nonmagnetic impurities, our result shows that this is not true for the side-jump conductivity of massive Dirac fermions that scatter off magnetic impurities. The reason is that, although the coordinate shift is responsible for both σ_{ij}^{sj} and σ_{ij}^{ad} , the interaction between magnetic impurities and massive Dirac fermions is anisotropic. Consequently, the transport of massive Dirac fermions during their side jump depends on the direction of the external electric field.

$\sigma_{ij}^{m.sj}$ (with $ij = xy$ and yx) is plotted against θ for some different values of m in panel (a) of Fig. 3 and also in terms of m for some different values of θ in panel (b) of this figure. In case of $\theta = 0$, $|\sigma_{xy}^{m.sj}| = |\sigma_{yx}^{m.sj}|$ and putting aside the sign of these conductivities, the system behaves isotropically relative to the external electric field direction. Increasing θ increases the magnitude of the corresponding transverse conductivity, and this is caused by the interplay between two factors. Firstly, the back-scattering probability is the main mechanism which suppresses both longitudinal and transverse conductivity. By increasing θ , the back-scattering probability $w^{(2,m)}(\mathbf{k}, -\mathbf{k}) \sim [(1 - \gamma_k^2) \sin^2 \theta \sin^2 \phi_k + \cos^2 \theta]$ decreases, so the transverse conductivity will increase. Secondly, the angular part of the magnetic side-jump velocity $[1 + 4 \sin^2 \phi_k (\sin^2 \theta + \sin^4 \theta)]^{1/2}$ increases with increasing θ and subsequently the conductivity increases. As it is clear from panel (b) of the figure, $\sigma_{ij}^{m.sj}$ is zero if we put the Fermi level exactly on the lowest state of the surface band structure ($m = 1$ or $\epsilon_F = M$). Beyond $m = 1$, $\sigma_{ij}^{m.sj}$ experiences a peak

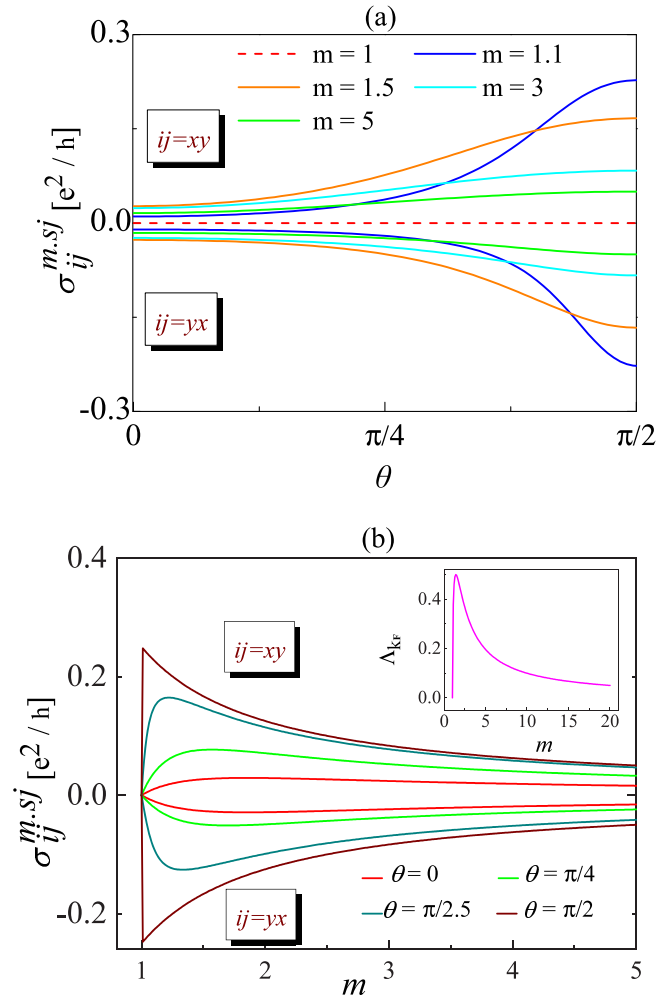


FIG. 3. $\sigma_{xy}^{m,sj}$ and $\sigma_{yx}^{m,sj}$ are plotted in terms of θ for some different values of m in (a), and in terms of m for some different values of θ in panel (b), respectively. In the inset of (b), Λ_{kF} is plotted against m . As it is clear from the main window of (b), $\sigma_{ij}^{m,sj}$ is inherited its nonmonotonic behavior from Λ_{kF} .

close to $m = 1$, and thereafter decreases by increasing m for all values of θ . This nonmonotonic feature of the conductivity arises from the nonangular part of the side-jump velocity (Λ_k) which has the same trend against m [as shown in inset of Fig. 3(b)]. Therefore deviating the system a bit from the insulating state or being far enough away from the perfect metallic state ($m \gg 1$ or $\mu \gg M$) can produce a large value for the side-jump conductivity.

To better understand the behavior of $\sigma_{ij}^{m,sj}$ and $\sigma_{ij}^{m,ad}$ in this section and also the behavior of other magnetic contributions to the AHE discussed in other sections, Fig. 4 is presented, which shows different effective mean free paths of the electrons as function of θ . The red and magenta curves in this figure represent $\tilde{\lambda}_{1,1}^{m,ad,s}(m, \theta) = \frac{\epsilon_F}{\hbar v_F} \lambda_{1,1}^{m,ad,s}$ and $\tilde{\lambda}_{1,1}^{m,s,c}(m, \theta) = \frac{n_{im}\epsilon_F J^2 S_m^2}{4\hbar^3 v_F^3} \lambda_{1,1}^{m,s,c}$ for $m = 1.5$ and $\mathbf{E} = E \hat{x}$. Based on Eq. (25), for the case that $\mathbf{E} = E \hat{x}$, one obtains $g_k^{m,ad} = eE \lambda_{1k}^{m,ad} \frac{\partial f^0}{\partial \epsilon_k}$ and $g_k^{m,s} = eE \lambda_{1k}^{m,s} \frac{\partial f^0}{\partial \epsilon_k}$. Furthermore (as shown in Appendixes A and B), among all terms in the Fourier expansion of $\lambda_{1k}^{m,ad}$

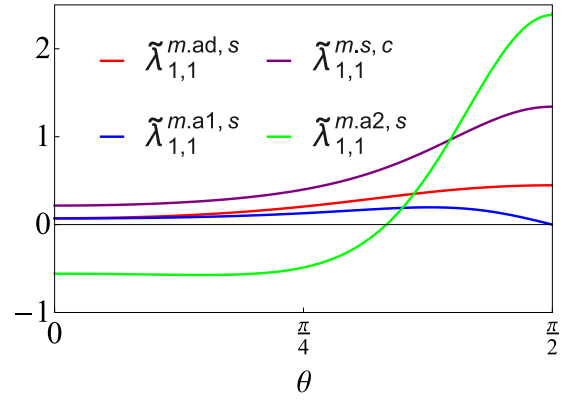


FIG. 4. Effective mean free path of electrons during different scattering events are plotted against θ for $m = 1.5$ and $\mathbf{E} = E \hat{x}$. $\tilde{\lambda}_{1,1}^{m,ad,s}$, $\tilde{\lambda}_{1,1}^{m,s,c}$, $\tilde{\lambda}_{1,1}^{m,a1,s}$, and $\tilde{\lambda}_{1,1}^{m,a2,s}$ are the effective mean free paths of electrons during a magnetic side-jump scattering, a magnetic longitudinal scattering, a conventional magnetic skew scattering and an intrinsic magnetic skew scattering, respectively.

and $\lambda_{1k}^{m,s}$ only $\lambda_{1,1}^{m,ad,s}$ and $\lambda_{1,1}^{m,s,c}$ determine the corresponding conductivity. As shown in Fig. 4, when θ increases from 0 to $\frac{\pi}{2}$, $\tilde{\lambda}_{1,1}^{m,ad,s}$ and $\tilde{\lambda}_{1,1}^{m,s,c}$ increase, which means an increase in the number of electrons participating in the magnetic side-jump scattering. Consequently this leads to an increase in the corresponding conductivities $\sigma_{yx}^{m,ad}$ and $\sigma_{yx}^{m,sj}$.

In addition, since $\sigma_{ij}^{m,sj} = \sigma_{ji}^{m,ad}$ we find $\sigma_{xy}^{tot,m,sj} = \sigma_{xy}^{m,sj} + \sigma_{yx}^{m,sj}$. Furthermore, as Fig. 3 shows $\sigma_{yx}^{m,sj} < 0$, then we can rewrite $\sigma_{xy}^{tot,m,sj} = |\sigma_{xy}^{m,sj}| - |\sigma_{yx}^{m,sj}|$. Finally since based on Fig. 5 always $\sigma_{xy}^{tot,m,sj} \geq 0$, we can conclude that $|\sigma_{xy}^{m,sj}| \geq |\sigma_{yx}^{m,sj}|$. This inequality surprisingly proves our already made prediction just based on looking at the profile of $\mathbf{v}_k^{m,sj}$. Figure 5 shows $\sigma_{ij}^{tot,m,sj}$ in terms of m for some values of θ in the main window and against θ for some different values of m in the inset. In this figure for two cases $\theta = 0$ and $\theta = \frac{\pi}{2}$, $\mathbf{J}^{m,ad}$ and $\mathbf{J}^{m,sj}$ cancel out each other and there is no net

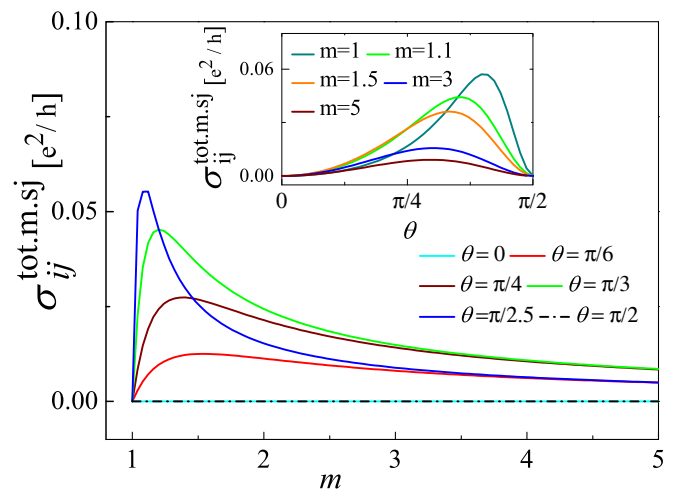


FIG. 5. $\sigma_{ij}^{tot,m,sj}$ is plotted in terms of m for some values of θ in the main panel, and in terms of θ for some different values of m in the inset.

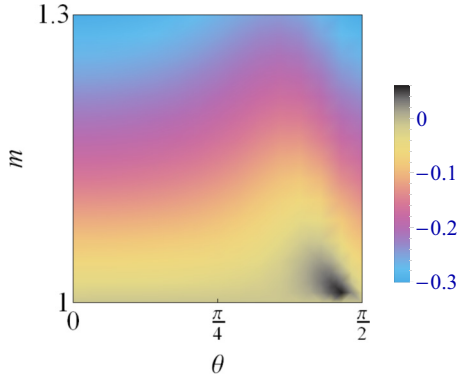


FIG. 6. $\sigma_{xy}^{\text{tot.sj}}$ is plotted in terms of θ and m .

conductivity due to the side-jump effect. Within $0 < \theta < \frac{\pi}{2}$, $\sigma_{ij}^{\text{tot.m.sj}}$ has a minimum value at $m = 1$, thereafter increases sharply within interval of $1 \leq m \lesssim 1.5$, until it reaches its maximum value. By further increasing m , the net side-jump conductivity decreases until it reaches zero in the limit of $m \rightarrow \infty$ or a gapless system. By changing the spatial orientation of the surface magnetization within $0 \leq \theta \leq \frac{\pi}{2}$ and also tuning the mass of the Dirac fermions, this contribution varies within $0 \leq \sigma_{ij}^{\text{tot.m.sj}}[m, \theta] < 0.07$. The small value of this contribution is caused by the fact that $\sigma_{ij}^{\text{m.sj}}$ and $\sigma_{ij}^{\text{m.ad}}$ partially cancel each other in $\sigma_{ij}^{\text{tot.m.sj}}$. In short, in order to have a maximal total side-jump conductivity arising from just magnetic impurities, we need to put the Fermi level just above the lowest state in the surface band structure and also tune the orientation of the surface magnetization within the interval $\frac{\pi}{3} < \theta < \frac{\pi}{2}$.

Finally, we consider the nonmagnetic scattering events, and using Eq. (39) we arrive at

$$\sigma_{xy}^{\text{tot.nm.sj}} = -\sigma_{yx}^{\text{tot.nm.sj}} = \frac{2(1-m^2)}{m(m^2+3)}, \quad (40)$$

where $\sigma_{ij}^{\text{tot.nm.sj}} = \sigma_{ij}^{\text{tot.nm.sj}} + \sigma_{ij}^{\text{tot.nm.ad}}$. These results also coincide with the ones reported in Ref. [34]. Thus also this contribution to the side-jump conductivity is isotropic (ignoring the sign difference). Figure 6 shows $\sigma_{xy}^{\text{tot.sj}}$ in terms of θ and m , where $\sigma_{xy}^{\text{tot.sj}} = \sigma_{xy}^{\text{tot.m.sj}} + \sigma_{xy}^{\text{tot.nm.sj}}$. As Fig. 6 shows, $\sigma_{xy}^{\text{tot.sj}}$ has a negligible sensitivity against θ . It can easily be verified that this is true also for $\sigma_{yx}^{\text{tot.sj}}$. Therefore, among the two different types of impurities, the nonmagnetic impurities contribution to the side-jump conductivity $\sigma_{ij}^{\text{tot.sj}}$ dominates.

We also want to stress that both $\sigma_{yx}^{\text{tot.m.sj}}$ and $\sigma_{yx}^{\text{tot.nm.sj}}$ have positive signs for all values of m and θ , hence $\sigma_{yx}^{\text{tot.sj}}$ is always positive. However, $\sigma_{xy}^{\text{tot.m.sj}}$ and $\sigma_{xy}^{\text{tot.nm.sj}}$ have opposite signs. Consequently, $\sigma_{xy}^{\text{tot.sj}}$ could change sign if one changes m or θ . Figure 6 shows this sign change at the boundaries of the black region in this figure.

Finally, notice that even though the concentration of impurities does not appear in the final expression for $\sigma_{ij}^{\text{tot.sj}}$, this contribution does originate from the presence of impurities. There are two parameters which play an important role in the transport of electrons during their side jump, the so called side-jump relaxation time and the side-jump velocity. The first one is inversely proportional to the concentration of impurities, though the second one is directly proportional to the concentration of impurities. Therefore, interestingly, their product is independent of the concentration of impurities.

3. Skew scattering

As we already indicated, skew scattering contributes to the AHE by two distinct terms. Here, we call the first term conventional skew scattering and the second term intrinsic skew scattering. The first term depends on the concentration of impurities and introduces g_k^{a1} in the distribution function f_k , and the other term which is independent of the concentration of impurities adds g_k^{a2} to f_k . Since we deal now with the intrinsic regime in which the first term is very negligible, we just keep the second term. The associated contribution to the second term is $\mathbf{J}^{sk2} = -e \sum_k g_k^{a2} \mathbf{v}_{0k}$. In order to find \mathbf{J}^{sk2} , we first need to calculate $w_{kk'}^{(4)}$ through Eq. (16) and then by solving Eq. (29) we find g_k^{a2} . Our result for both kinds of impurities are

$$w_{kk'}^{(4, nm)} = \frac{3M\pi (n_{\text{inm}} V_0^2)^2}{4\hbar} \frac{k^2}{\varepsilon_k^3} \sin \alpha_k \delta(\varepsilon_k - \varepsilon_{k'}), \quad (41)$$

$$w_{kk'}^{(4, m)} = w_0^{(4)} \gamma [(\gamma^2 - 1) \cos 2\theta (\sin \phi_k \cos \phi_{k'} - \sin \alpha_k) + \gamma \sqrt{1 - \gamma^2} \sin 2\theta (2 \sin \phi_k - \sin \phi_{k'}) - (\gamma^2 - 1) (\sin \alpha_k + \sin \phi_{k'} \cos \phi_k)], \quad (42)$$

with $\alpha_k = \phi_{k'} - \phi_k$ and $w_0^{(4)} = \frac{\pi (n_{\text{inm}} J^2 S_m^2)^2}{4\hbar^3 v_F^2} \delta(\varepsilon_k - \varepsilon_{k'})$. Inserting these scattering rates in Eq. (29) and using the already found $w_{kk'}^{(2, m)}$ and g_k^s expressions, we obtain the following transverse conductivities associated to scattering off magnetic and nonmagnetic impurities (for more information see Appendix D):

$$\sigma_{xy}^{m.sk2} = \frac{16(g-2)[m^2-1](-\cos 4\theta + (m^2+2)\cos 2\theta + 2m^2+2)}{m([g+2]\cos 2\theta + [g+4]m^2-2)(g\cos 4\theta + 2[g-2]m^2\cos 2\theta + g-4)}, \quad (43)$$

$$\sigma_{yx}^{m.sk2} = \frac{4(g-2)(b\cos 2\theta - g[2(g+1)m^4 + g-2] - [g-2][g+2m^2]\cos 4\theta + 8m^4 - 4m^2 + 8)}{gm([g+2m^2]\cos 2\theta + [g+2]m^2)([g-2][\cos 2\theta + m^2] + \cos 4\theta - 1)}, \quad (44)$$

$$\sigma_{xy}^{nm.sk2} = -\sigma_{yx}^{nm.sk2} = -\frac{3(m^2-1)^2}{2m(m^2+3)^2}, \quad (45)$$

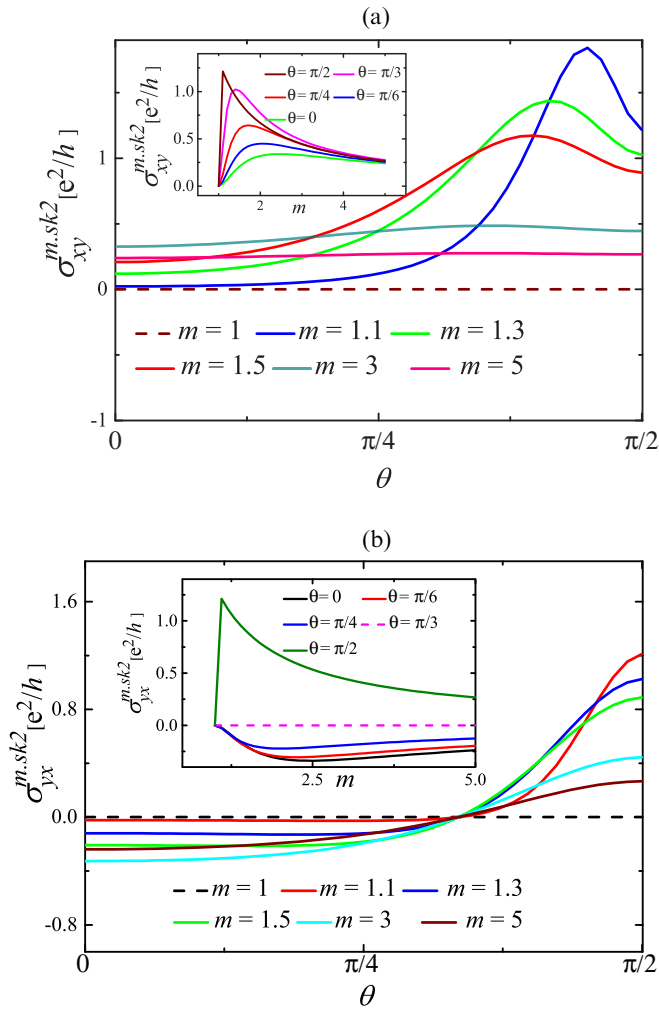


FIG. 7. $\sigma_{xy}^{m.sk2}$ is plotted in terms of θ for some different values of m in the main window of (a), and against m for some different values of θ in the inset of this panel. $\sigma_{yx}^{m.sk2}$ is plotted in (b) for the same choice of parameters θ and m .

with $b = 2[(-2g^2 + g + 8)m^2 - 2gm^4 + g]$. Note that $\sigma_{ij}^{m.sk2} = 0$ for the case $m = 1$ (the insulating regime) or in the limit of large m (the perfect metallic regime). To study $\sigma_{ij}^{m.sk2}$, Eq. (43) and (44) are illustrated in panels (a) and (b) of Fig. 7, respectively. As it is clear from panel (a), $\sigma_{xy}^{m.sk2}$ increases with increasing θ for all values of m , and reaches a maximum in the interval $\frac{\pi}{4} < \theta < \frac{\pi}{2}$. The inset of panel (a) shows $\sigma_{xy}^{m.sk2}$ as function of m for some values of θ . Each curve in this inset shows a maximum value in the interval $1 \leq m \leq 2$, followed by a sharp decrease. Panel (b) of this figure shows $\sigma_{yx}^{m.sk2}$ as function of θ for some values of m . The inset of this panel shows $\sigma_{yx}^{m.sk2}$ as function of m for some values of θ . Surprisingly $\sigma_{yx}^{m.sk2}$ is negative for $0 \leq \theta < \frac{\pi}{3}$ and has a positive value for $\frac{\pi}{3} < \theta \leq \frac{\pi}{2}$. This contribution changes sign if one changes the spatial orientation of the surface magnetization from 0 to $\frac{\pi}{2}$. The inset of this figure shows that, for all given values of θ , $|\sigma_{yx}^{m.sk2}|$ starts from zero at $m = 1$, then increases till it reaches a maximum value within the interval $1 \leq m \leq 2$, after which it decreases. Also in agreement with the main window of panel (b) which shows

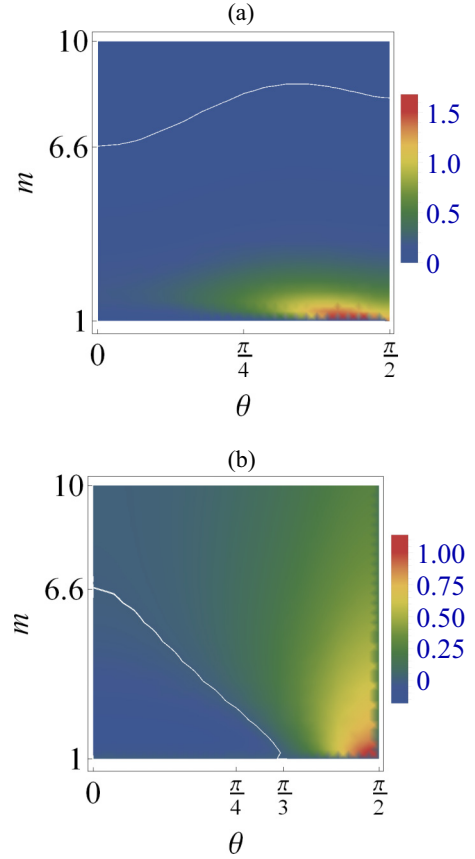


FIG. 8. $\sigma_{xy}^{tot.sk2}$ and $\sigma_{yx}^{tot.sk2}$ as functions of θ and m , are plotted in (a) and (b), respectively.

that the conductivity at $\theta = \frac{\pi}{2}$ is positive for all values of m , the green curve in the inset is positive for all values of m .

The observed sign change in $\sigma_{yx}^{m.sk2}$ can be understood from Eq. (23), which is a consequence of the principle of *detailed balance*, along with the conservation of the number of particles, which leads to $\sum_k (g_k^s + g_k^{ad} + g_k^{a1} + g_k^{a2}) = 0$. To fulfill these two constraints, the corresponding effective mean free path $\tilde{\lambda}_{1,1}^{m.a2,s} = \frac{\epsilon_F}{\hbar v_F} \lambda_{1,1}^{m.a2,s}$ in g_k^{a2} (see Appendix D), changes sign, as shown by the green curve in Fig. 4. Since $\lambda_{1,1}^{m.a2,s}$ is the only parameter involved in $\sigma_{yx}^{m.sk2}$ that depends on θ , the observed sign change of $\sigma_{yx}^{m.sk2}$ is totally inherited from this effective mean free path. Therefore, since each scattering process should be compensated by its reverse process and the external electric field should not alter the total number of residing electrons in the allowed states, $\sigma_{yx}^{m.sk2}$ has to change sign.

Finally, we consider the contribution due to the spin independent intrinsic skew scattering to the AHE, given in Eq. (45). This expression indicates that this conductivity is isotropic and also like $\sigma_{ij}^{m.sk2}$ it disappears for large values of m .

We have now obtained the conductivities $\sigma_{ij}^{m.sk2}$ and $\sigma_{ij}^{nm.sk2}$, which combined yield the total intrinsic skew scattering $\sigma_{ij}^{tot.sk2} = \sigma_{ij}^{m.sk2} + \sigma_{ij}^{nm.sk2}$. $\sigma_{xy}^{tot.sk2}$ and $\sigma_{yx}^{tot.sk2}$ are illustrated respectively in panels (a) and (b) of Fig. 8, in terms of θ and m . The white lines in these two panels specify the (θ, m) combinations for which the corresponding conductivity

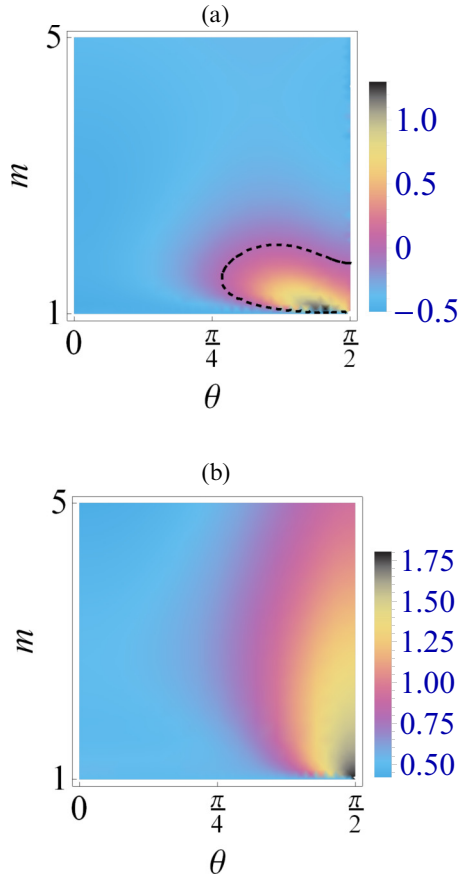


FIG. 9. $\sigma_{xy}^{\text{int.AHE}}[\theta, m]$ and $\sigma_{yx}^{\text{int.AHE}}[\theta, m]$ are plotted in (a) and (b), respectively.

is zero. Panels (a) and (b) show that, for $1 < m \lesssim 2$, $\sigma_{xy}^{\text{tot.sk}2}$ and $\sigma_{yx}^{\text{tot.sk}2}$ undergo a considerable change with respect to θ . Putting the Fermi level just above the gap and also aligning the surface magnetization close to the surface of the TI ($\frac{\pi}{3} \lesssim \theta \lesssim \frac{\pi}{2}$) causes the system to reach its maximum value for $\sigma_{ij}^{\text{tot.sk}2}$. It is also clear from panel (a) that there is just a small (θ, m) region with a significant $\sigma_{xy}^{\text{tot.sk}2}$, while in panel (b) a broad region shows a significant conductivity $\sigma_{yx}^{\text{tot.sk}2}$.

4. Total AHE in the intrinsic regime

After devoting Secs. III A 1–III A 3 to the different contributions to the AHE in the intrinsic regime, we are ready to discuss $\sigma_{ij}^{\text{int.AHE}} = \sigma_{ij}^{\text{an}} + \sigma_{ij}^{\text{tot.sj}} + \sigma_{ij}^{\text{tot.sk}2}$. The result is illustrated in Fig. 9. Based on this figure, we observe that $\sigma_{ij}^{\text{int.AHE}}$ is anisotropic. The black dashed line in panel (a) of Fig. 9 indicates the (m, θ) combinations for which $\sigma_{xy}^{\text{int.AHE}}[m, \theta] = 0$. Accordingly, tuning (m, θ) around this dashed line leads to a sign change in $\sigma_{xy}^{\text{int.AHE}}$. As it is clear from panel (b) of this figure, $\sigma_{yx}^{\text{int.AHE}}$ has always a persistent positive sign against any change in θ or m . Also, note that like the contribution of the intrinsic skew scattering, tuning the Fermi level just above the gap and also aligning the magnetization close to the surface, the maximum value for both components $\sigma_{xy}^{\text{int.AHE}}$ and $\sigma_{yx}^{\text{int.AHE}}$ is attained. At the end of this section, we consider two special magnetization orientations $\theta = 0$ and $\frac{\pi}{2}$. The

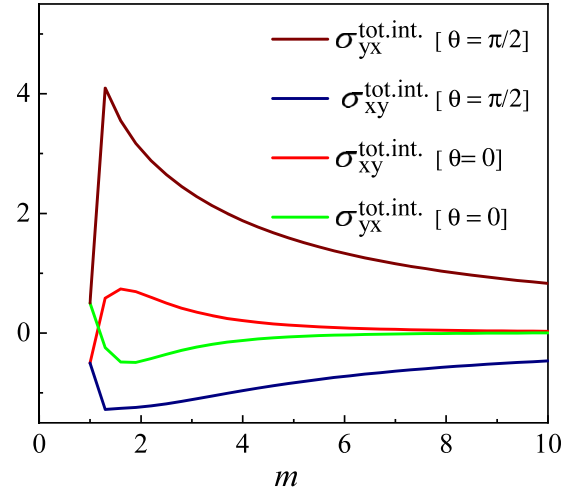


FIG. 10. $\sigma_{ij}^{\text{int.AHE}}$ is plotted as function of m for two values of $\theta = 0$ and $\frac{\pi}{2}$.

total intrinsic anomalous Hall conductivities corresponding to these two important cases are

$$\sigma_{xy}^{\text{int.AHE}}[\theta = 0] = \frac{m^6 + 95m^4 + 79m^2 - 207}{2(m^2 + 3)^2(3m^3 + m)}, \quad (46)$$

$$\sigma_{yx}^{\text{int.AHE}}[\theta = 0] = \frac{m^6 - 81m^4 - 49m^2 + 225}{2(m^2 + 3)^2(3m^3 + m)}, \quad (47)$$

$$\sigma_{xy}^{\text{int.AHE}}\left[\theta = \frac{\pi}{2}\right] = -\frac{29m^4 + 54m^2 + 45}{6m(m^2 + 3)^2}, \quad (48)$$

$$\sigma_{yx}^{\text{int.AHE}}\left[\theta = \frac{\pi}{2}\right] = \frac{17m^4 + 62m^2 + 81}{2m(m^2 + 3)^2}. \quad (49)$$

Above expressions are shown in Fig. 10. According to this figure, the anomalous Hall conductivity of the system with in-plane magnetization in the intrinsic regime is much larger than the conductivity of the same system and in the same regime with fully out-of-plane magnetization. For a system with fully out of plane easy axis magnetization ($\theta = 0$) and Fermi level close to the bottom of conduction band, the skew scattering contribution is negligible and the other two contributions control the AHE with comparable size. For the same system but with in-plane easy axis magnetization ($\theta = \frac{\pi}{2}$), surprisingly the contribution arising from skew scattering dominates the AHE. Remarkably, all contributions to the AHE in this regime vanish for a system in the fully metallic state (i.e., a large value of m), whatever the value of θ .

B. The extrinsic regime

According to our classification in Eq. (30), two terms control the AHE. As we already explained, $\sigma_{ij}^{\text{int.AHE}}$ is negligible against $\sigma_{ij}^{\text{ext.AHE}}$ in the extrinsic regime. Then neither the Berry-phase curvature nor the side jump play a role in $\sigma_{ij}^{\text{ext.AHE}}$, and the skew scattering is the only involved effect to the AHE in this regime, by its conventional component $\mathbf{J}^{\text{sk}1} = \sum_k \mathbf{v}_{0k} g_k^{\text{sk}1}$. Since $g_k^{\text{sk}1}$ is inversely proportional to the concentration of the impurities, $\sigma_{ij}^{\text{tot.sk}1} = \sigma_{ij}^{\text{ext.AHE}}$ dominates the AHE in a very dilute regime. From Eq. (15), we obtain

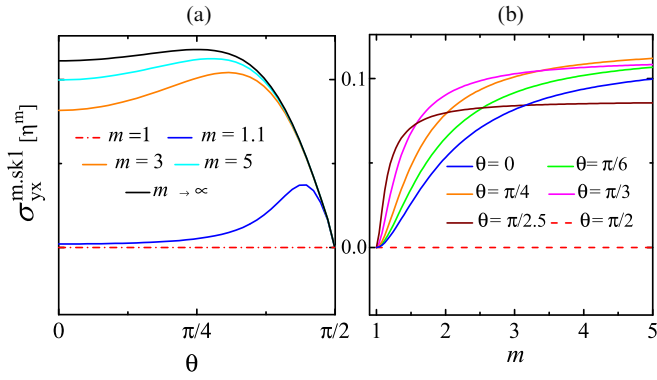


FIG. 11. $\sigma_{yx}^{m,sk1}$ is plotted in terms of θ and m in (a) and (b), respectively.

$w_{kk'}^{(3a,m)}$ for a magnetic scattering event and $w_{kk'}^{(3a,mm)}$ for a nonmagnetic scattering event

$$w_{kk'}^{(3a,m)} = w_0^{(3a,m)} \cos \theta \sin \alpha_k, \quad (50)$$

$$w_{kk'}^{(3a,mm)} = w_0^{(3a,mm)} \sin \alpha_k, \quad (51)$$

with $w_0^{(3a,m)} = -\frac{\pi n_{\text{im}} J^3 S_m^3 k^2}{2\hbar \varepsilon_k} \delta(\varepsilon_k - \varepsilon_{k'})$ and $w_0^{(3a,mm)} = -\frac{\pi n_{\text{im}} V_0^3 M k^2}{2\hbar \varepsilon_k^2} \delta(\varepsilon_k - \varepsilon_{k'})$. The factor $\cos \theta$ in the above expression implies that the z component of magnetization is responsible for the conventional skew scattering in our system. In addition the factor $\sin \alpha_k$ shows that the corresponding event is asymmetric under the exchange of indexes $\mathbf{k} \leftrightarrow \mathbf{k}'$. The result for nonmagnetic scatterers, Eq. (51), is again in agreement with the literature (see Eq. (70) in Ref. [34]). Substituting $w_{kk'}^{(3a,m)}$ in Eq. (28) gives us the corresponding mean free paths $\lambda_i^{m,a1}(\mathbf{k})$ ($i = 1, 2$), from which we obtain the distribution function $g_k^{m,a1}$ using Eq. (25), and subsequently the following corresponding conductivity for scattering off magnetic impurities (for more details see Appendix C):

$$\sigma_{xy}^{m,sk1} = \frac{D(2-g)(\cos 2\theta + m^2)}{(g \cos 4\theta + 2(g-2)m^2 \cos 2\theta + g-4)}, \quad (52)$$

with $D = \eta_1^m \frac{4(m^2-1) \cos \theta}{(g+2) \cos 2\theta + (g+4)m^2 - 2}$, $\eta_1^m = \frac{\mu}{n_{\text{im}} S_m J}$. Also, we show that $\sigma_{yx}^{m,sk1} = -\sigma_{xy}^{m,sk1}$.

In panel (a) of Fig. 11, $\sigma_{yx}^{m,sk1}[\eta^m]$ is shown against θ for some values of m . This figure shows that $\sigma_{yx}^{m,sk1}$ smoothly increases for increasing θ , until it reaches a maximum in the interval $\frac{\pi}{4} < \theta < \frac{\pi}{2}$. Thereafter it sharply decreases until it vanishes at $\theta = \frac{\pi}{2}$. Panel (b) shows that putting the surface of the system into the insulator regime, i.e., $m = 1$, turns off the transverse conductivity $\sigma_{yx}^{m,sk1}$, regardless of the orientation of the magnetization. For larger values of m , $\sigma_{yx}^{m,sk1}$ increases with increasing m . In addition, as shown by the black curve in panel (a), the conductivity saturates at $\sigma_{yx}^{m,sk1}(m \rightarrow \infty) = \eta_1^m \frac{\cos \theta}{6+3 \cos 2\theta}$ for very large values of m . Thus by closing the gap or driving the system into a perfect metallic regime, conventional skew scattering still has a nonzero contribution in the conductivity of the system. This feature reveals one of the main differences between the magnetic skew scattering

contribution and the other contributions which vanish in a gapless system or in the perfect metallic regime.

Since the conductivity of electrons during conventional magnetic skew scattering depends on \mathbf{v}_{0k} and $g_k^{m,a1}$ (see Appendix C), its behavior with respect to θ can be easily traced by looking at the behavior of \mathbf{v}_{0k} and $g_k^{m,a1}$ against θ . As \mathbf{v}_{0k} is independent of θ , studying $g_k^{m,a1}$ against θ is sufficient for this purpose. Considering that $\sigma_{yx}^{m,sk1} = -\sigma_{xy}^{m,sk1}$, we just discuss the distribution function associated to $\sigma_{yx}^{m,sk1}$, $g_k^{m,a1} = eE \lambda_{1k}^{m,a1} \frac{\partial f^0}{\partial \varepsilon_k}$. Among all terms in the Fourier expansion of $\lambda_{1k}^{m,a1}$, we just need to discuss effective term $\tilde{\lambda}_{1,1}^{m,a1,s} = \frac{J n_{\text{im}} S_m}{\hbar v_F} \lambda_{1,1}^{m,a1,s}$. The curve corresponding to this term is the blue curve in Fig. 4. This curve shows that when θ increases, $\tilde{\lambda}_{1,1}^{m,a1,s}$ and consequently the number of electrons participating in the conventional magnetic skew scattering increase very smoothly, and decrease again after a certain value of θ , and further turn off at the $\theta = \frac{\pi}{2}$. Accordingly, as Fig. 11 confirms, the contribution of the magnetic conventional skew scattering to the AHE $\sigma_{yx}^{m,sk1}$ has the same trend of $\tilde{\lambda}_{1,1}^{m,a1,s}$ against θ .

Repeating the same calculations for the conventional skew scattering contribution due to scattering of nonmagnetic impurities, we obtain the following expression for the conductivity:

$$\sigma_{yx}^{nm,sk1} = -\sigma_{xy}^{nm,sk1} = \eta_1^{nm} \frac{(m^2 - 1)^2}{m(m^2 + 3)(5 + 3m^2)}, \quad (53)$$

with $\eta_1^{nm} = \frac{\mu}{n_{\text{im}} V_0}$. The minimum value of $|\sigma_{ij}^{nm,sk1}[m]|$ is obtained in those systems with the Fermi level just above the bottom of the conduction band, and the maximum value is reached in a system with $m = 3.5$. Equation (53) does not coincide completely with Eq. (72) in Ref. [34], which might be due to an extra approximation that is made in Ref. [34]. Like all the previously discussed contributions, this contribution is zero for an insulating surface $m = 1$. In contrast to $\sigma_{ij}^{m,sk1}$, this contribution is absent in the perfect metallic regime $m \rightarrow \infty$. Since $\sigma_{ij}^{\text{tot},sk1} = \sigma_{ij}^{m,sk1} + \sigma_{ij}^{nm,sk1} = -\sigma_{ji}^{\text{tot},sk1}$, we just discuss $\sigma_{yx}^{\text{tot},sk1}$ in the remaining part. Figure 12 shows $\sigma_{yx}^{\text{tot},sk1}[\eta_1^{nm}]$ in terms of θ and m for two different values of $\nu = \frac{\eta_1^m}{\eta_1^{nm}}$, $\nu = 0.1$ and $\nu = 100$ in panels (a) and (b), respectively, for the particular case of $n_{\text{im}} = n_{\text{imm}}$. It shows that increasing m increases $\sigma_{yx}^{\text{tot},sk1}$, while increasing ν decreases this conductivity. In addition, this contribution becomes insignificant for small values of m , independent of the value of ν and θ .

Also note that, in contrary to the total contribution of the side jump and intrinsic skew scattering, the total contribution

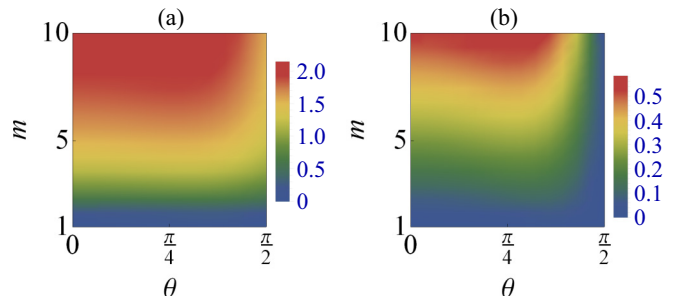


FIG. 12. $\sigma_{yx}^{\text{tot},sk1}[\eta^{nm}]$ is plotted in terms of θ and m for $\nu = 0.1$ and $\nu = 100$ in (a) and (b), respectively.

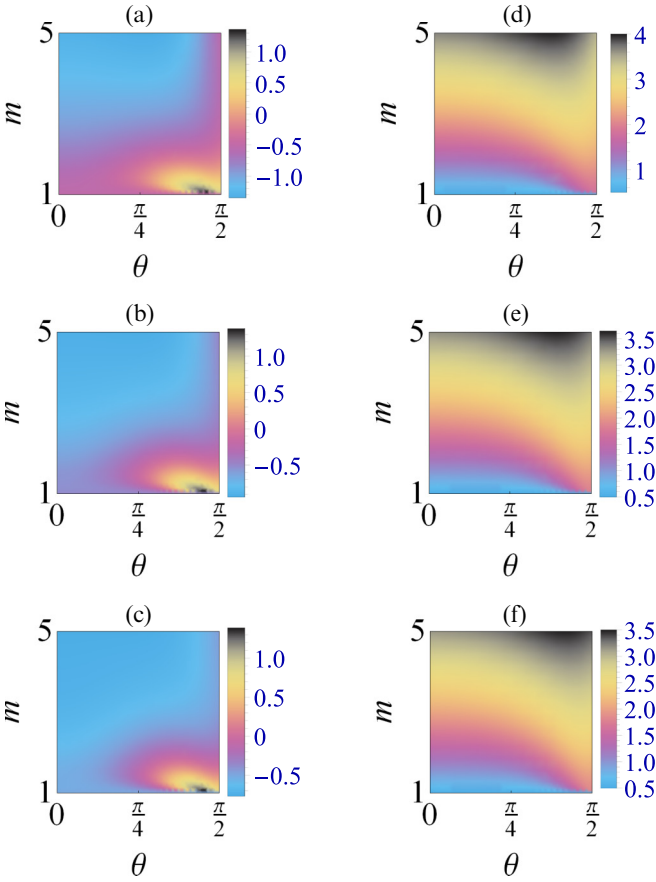


FIG. 13. σ_{xy}^{AHE} and σ_{yx}^{AHE} are plotted respectively in the first and second columns, in terms of θ and m , for some values of n_{im} . First, second, and third rows correspond to $n_{\text{im}} = 0.4, 0.7$ and 1 , respectively.

of the conventional skew scattering never changes its sign, whatever the value of θ , m or E .

There is some experimental and theoretical evidences that the surface magnetization of a TI is preferentially orientated in the plane of the surface or perpendicular to it [31,53]. For these orientations, $\theta = 0$ and $\frac{\pi}{2}$, $\sigma_{yx}^{\text{tot.sk1}}[\eta_1^{nm}]$ is given by

$$\sigma_{yx}^{\text{tot.sk1}}[\theta = 0] = -\frac{\nu - \nu m^2}{3m^2 + 1} + \frac{m^4 - 2m^2 + 1}{3m^5 + 14m^3 + 15m}, \quad (54)$$

$$\sigma_{yx}^{\text{tot.sk1}}\left[\theta = \frac{\pi}{2}\right] = \frac{(m^2 - 1)^2}{2(3m^4 + 14m^2 + 15)}. \quad (55)$$

Investigations of the above expressions show that $\sigma_{yx}^{\text{tot.sk1}}[\theta = 0]$ does not vary much against m for small values of ν . However, for large ν values, it undergoes a large change with respect to m . Moreover, since the magnetic skew scattering of the Fermi electrons has no contribution to the AHE in a system with in-plane magnetization, the $\sigma_{yx}^{\text{tot.sk1}}[\theta = \frac{\pi}{2}]$ does not change with ν .

C. The intermediate regime

In this regime, extrinsic and intrinsic terms both contribute to the AHE with comparable sizes. Figure 13 is shown to discuss the behavior of the conductivity σ_{ij}^{AHE} in terms of θ and m

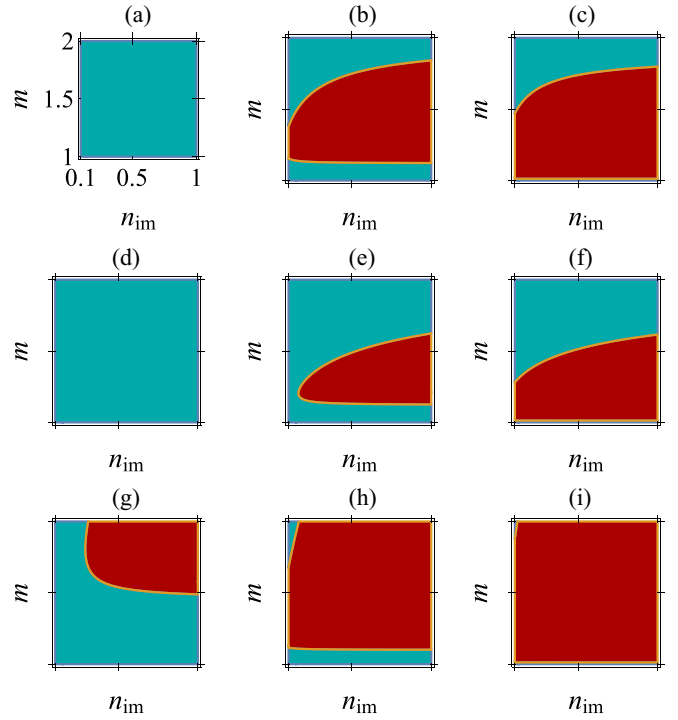


FIG. 14. σ_{xy}^{AHE} is plotted in terms of n_{im} and m for some values of θ and ν . The blue part corresponds to negative values of σ_{xy}^{AHE} and the red part corresponds to positive values. The first, second, and third rows correspond to $\nu = 10, 0.1$, and 0 , respectively. Also, first, second and third column correspond to $\theta = \frac{\pi}{6}, \frac{\pi}{3}$, and 0.44π , respectively.

for some values of $n_{\text{im}} (=n_{\text{inm}})$ at an arbitrary $\nu = \frac{\eta_1^m}{\eta_1^{nm}} = 0.83$. The first column of this figure illustrates how σ_{xy}^{AHE} behaves against θ and m for $n_{\text{im}} = 0.4, 0.7$, and 1 in panels (a), (b), and (c), respectively. In the second column, σ_{yx}^{AHE} is shown for the same choices of n_{im} . As it is shown in panels (a), (b), and (c) there is a crossover from the positive values to the negative values for the corresponding conductivity. In addition, the maximum value of σ_{xy}^{AHE} occurs if we place the Fermi level close to the bottom of the conduction band and also adjust the surface magnetization close to $\frac{\pi}{2}$. Surprisingly, in contrast to σ_{xy}^{AHE} , the second column illustrates that σ_{yx}^{AHE} is always positive. This term in panel *d, e* and *f* gets its maximum value for large values of m (close to 5) and a magnetization within $\frac{\pi}{4} \leq \theta \leq \frac{\pi}{2}$. Then, although these two components of σ_{ij}^{AHE} behave differently respect to given parameters, they share this feature that they get their maximum value around $\theta \simeq \frac{\pi}{2}$.

Moreover, as all panels in Fig. 14 except panels (a) and (d) show, σ_{xy}^{AHE} undergoes a sign change with respect to n_{im} . This sign change in the anomalous Hall conductivity has recently been observed experimentally [31]. Remarkably, for specific impurity concentrations, the AHE can two times undergo a sign change by increasing the Fermi level m , as panels (b) and (e) of Fig. 15 show. This interesting sign change of the AHE is inherited from the nonmonotonic behavior of all the contributions to the AHE. In addition, this nonmonotonic behavior of the AHE distinguishes it from the corresponding reported longitudinal conductivity [52].

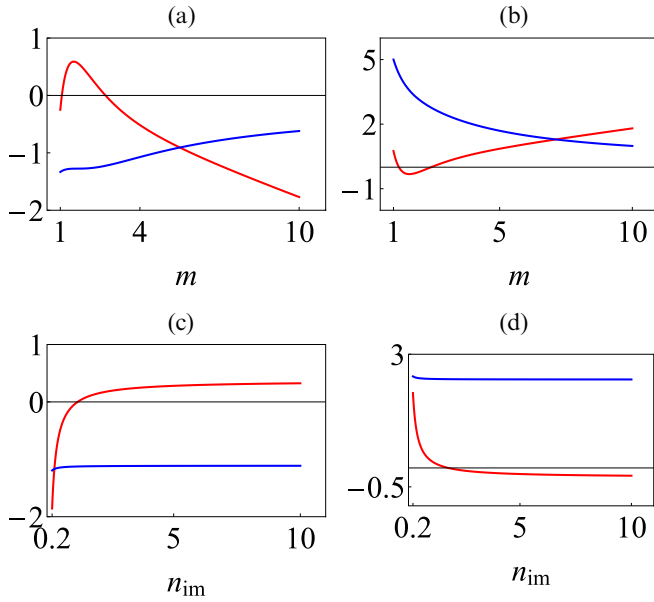


FIG. 15. σ_{xy}^{AHE} and σ_{yx}^{AHE} are plotted in the first and the second columns, respectively. In the first row, these conductivities are plotted against m for $n_{\text{im}} = n_{\text{imm}} = 1$ and $\nu = 1$, and in the second row, against n_{im} for $m = 3$ and $\nu = 1$. The red and blue curves correspond to the cases $\theta = 0$ and $\frac{\pi}{2}$, respectively. It is clear that, in contrast to the case $\theta = \frac{\pi}{2}$, sign changes occur with respect to m or n_{im} for $\theta = 0$.

Finally, like in previous sections, we briefly discuss the two cases $\sigma_{ij}^{\text{AHE}}[\theta = 0]$ and $\sigma_{ij}^{\text{AHE}}[\theta = \frac{\pi}{2}]$. All red curves in Fig. 15, corresponding to $\sigma_{ij}^{\text{AHE}}[\theta = 0]$ undergo a sign change via changing m or n_{im} , in contrary to $\sigma_{ij}^{\text{AHE}}[\frac{\pi}{2}]$ (blue curve) which does not show such a sign change. Therefore, since the AHE in this regime is very anisotropic, observing its sign change with respect to m or n_{im} , requires properly adjusting all the involved parameters, the direction of external electric field, the orientation of the surface magnetization, the position of the Fermi level, the concentration of the impurities and also the ratio of the nonmagnetic scattering potential to the magnetic scattering potential.

In addition, note that in the absence of magnetic impurities, we can write the total AHE as

$$\sigma_{ij}^{\text{AHE}} = \sigma_{ij}^{\text{an}} + \sigma_{ij}^{\text{tot.nm.sj}} + \sigma_{ij}^{\text{nm.sk1}} + \sigma_{ij}^{\text{nm.sk2}}. \quad (56)$$

For $ij = xy$, one can show, based on Eqs. (32), (40), (53), and (45), that $\sigma_{xy}^{\text{an}} < 0$, $\sigma_{xy}^{\text{tot.nm.sj}} < 0$, $\sigma_{xy}^{\text{nm.sk1}} < 0$ and $\sigma_{xy}^{\text{nm.sk2}} < 0$. Obviously, in the absence of magnetic impurities $\sigma_{xy}^{\text{AHE}} < 0$ for all $m \geq 1$. For $ij = yx$, considering that $\sigma_{yx}^{\text{an}} = -\sigma_{xy}^{\text{an}}$, $\sigma_{yx}^{\text{tot.nm.sj}} = -\sigma_{xy}^{\text{tot.nm.sj}}$, $\sigma_{yx}^{\text{nm.sk1}} = -\sigma_{xy}^{\text{nm.sk1}}$, and $\sigma_{yx}^{\text{nm.sk2}} = -\sigma_{xy}^{\text{nm.sk2}}$, it is clear that in the absence of magnetic impurities $\sigma_{yx}^{\text{AHE}} > 0$ for all $m \geq 1$. Therefore we can conclude that, in the presence of just nonmagnetic impurities, the AHE never undergoes a sign change, whatever the direction of \mathbf{E} . The absence of this sign change in the AHE in a system with only nonmagnetic impurities has been already reported in both the noncrossing [34] as the crossing regime [35].

Table I and Fig. 16 help us to figure out the story behind the observed sign changes in this and previous sections. In

TABLE I. The signs of the different contributions to the AHE are summarized. $\mathbf{E} = E\hat{x}$ is perpendicular to the plane of the surface magnetization (yz plane) and $\mathbf{E} = E\hat{y}$ is parallel to the plane of the surface magnetization.

Sign of the different contributions to the AHE								
Electric field	σ_{ij}^{in}	$\sigma_{ij}^{\text{tot.m.sj}}$	$\sigma_{ij}^{\text{tot.nm.sj}}$	$\sigma_{ij}^{\text{m.sk1}}$	$\sigma_{ij}^{\text{nm.sk1}}$	$\sigma_{ij}^{\text{m.sk2}}$	$\sigma_{ij}^{\text{nm.sk2}}$	AHE
$\mathbf{E} = E\hat{x}$	+	+	+	+	+	+, -	+	+
$\mathbf{E} = E\hat{y}$	-	+	-	-	-	+	-	+, -

case the external electric field is exerted perpendicular to the plane of the surface magnetization, all contributions to the AHE have a positive sign, except the one produced by the magnetic intrinsic skew scattering $\sigma_{ij}^{\text{m.sk2}}$ which, depending on (m, θ) can have a positive or negative sign. When the external electric field is exerted parallel to the plane of the surface magnetization, all contributions to the AHE have negative sign, except those arising from the magnetic side-jump and the magnetic intrinsic skew scattering. In the first case (i.e., the electric field is along \hat{x}), $\sigma_{yx}^{\text{m.sk2}}$ has a negative sign only within $0 \leq \theta \leq \frac{\pi}{3}$, as also shown in Fig. 7. However, since this negative value is insignificant compared to the sum of the positive terms, the anomalous Hall conductivity always has a persistent positive sign against (m, θ) , if $\mathbf{E} = E\hat{x}$. Regarding the second case (i.e., the electric field is along \hat{y}), all involved mechanisms contribute to the AHE with negative

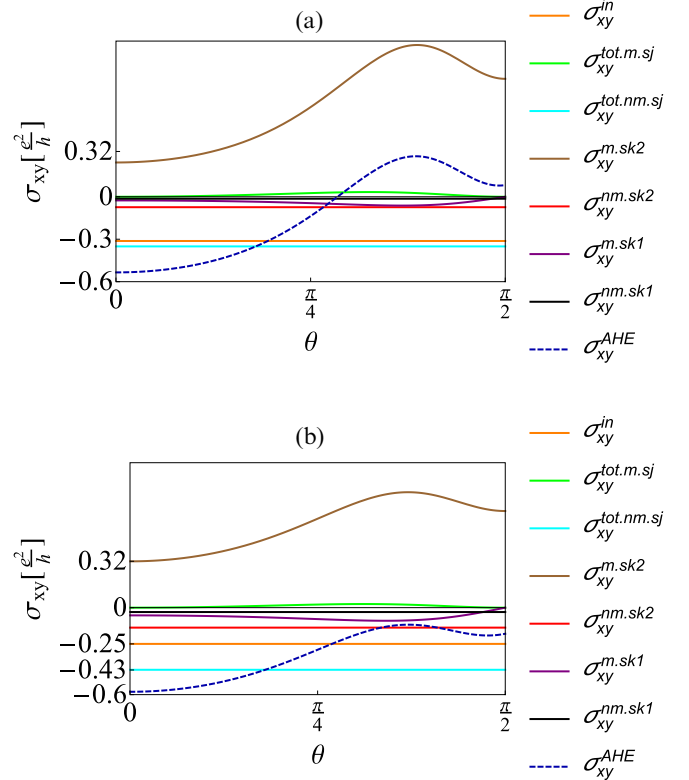


FIG. 16. All contributions to the AHE (solid lines) and the total conductivity (dashed line), plotted against θ . In (a), $m = 1.6$, $n_{\text{im}} = n_{\text{imm}} = 1$, $\eta_1^m = \eta_1^{\text{nm}} = 0.8$ and in (b), $m = 2$, $n_{\text{im}} = n_{\text{imm}} = 1$, $\eta_1^m = \eta_1^{\text{nm}} = 1$.

sign except the magnetic side-jump and the magnetic intrinsic skew scattering. Accordingly, depending on the value of m , θ , η_1^m , and η_1^{mm} , the anomalous Hall conductivity can have a negative or positive sign. In order to produce an anomalous Hall current with persistent sign against any change in θ , m , η_1^m , and η_1^{mm} , either the sum of the terms with negative sign or the sum of the terms with positive sign should dominate the AHE.

An example is shown in Fig. 16. In panel (a), the significant positive component $\sigma_{xy}^{m.sk2}$ is large enough to overwhelm the sum of the negative contributions and finally imposes a sign change in σ_{xy}^{AHE} via tuning θ around $\frac{\pi}{4}$. Though, if we just increase m from $m = 1.6$ [in panel (a)] to $m = 2$ [in panel (b)] and keep the other variables unchanged, the relative importance of $\sigma_{xy}^{m.sk2}$ weakens and eventually leads to the appearance of the AHE with a persistent negative sign, as shown in panel (b) of this figure.

IV. SUMMARY

In this work, the anomalous Hall conductivity of a 3D TI is investigated systematically using the semiclassical Boltzmann approach along with a modified relaxation time scheme, in terms of the Fermi level (ε_F) and the band gap ($2M$), the spatial orientation of the surface magnetization θ (an orientation perpendicular to the surface corresponds to $\theta = 0$, an orientation in the \hat{y} direction to $\theta = \frac{\pi}{2}$) and also the concentration of magnetic and nonmagnetic impurities. There are three contributions to the AHE, namely, the intrinsic effect (arising from a nonzero Berry curvature), the side-jump effect and the skew scattering effect. They are competing to dominate the anomalous hall conductivity of the system. In this work by applying a fully analytical method we investigate how the spatial orientation of the surface magnetization and also the value of $m = \varepsilon_F/M$ influence the transport of the massive Dirac fermions on the surface of a 3D TI, doped with static point like, randomly placed, magnetic and nonmagnetic impurities. Since the contribution of nonmagnetic impurities to the AHE has been investigated by others before [34], here we mainly focus on the effect of magnetic impurities to the AHE. Concerning the side-jump contribution, by tuning the surface magnetization near the surface of the TI and also putting the Fermi level just above the bottom of the conduction band, one can turn off and on the total side-jump contribution in the presence of both kinds of impurities. Next, the contributions coming from conventional and intrinsic skew scattering are investigated. In contrary to the total magnetic side-jump contribution, which vanishes in a fully metallic regime, the conductivity corresponding to magnetic conventional skew scattering surprisingly gets its maximal value in this regime. However, similar to the side-jump magnetic contribution, it disappears in a system with in-plane magnetization. In the presence of nonmagnetic impurities, the total contribution of the conventional skew scattering is still isotropic, and in the metallic regime it reaches a significant value if the magnetization is out of plane. In addition, the skew scattering effect contributes to the AHE through an additional correction, called the intrinsic term. Our results

show that, despite the previous conventional contribution, this contribution does not vanish at $\theta = \frac{\pi}{2}$. Besides, this intrinsic contribution disappears at the fully metallic regime, just like the side-jump contribution. Remarkably, by applying an external electric field perpendicular to the in-plane component of the magnetization, and tuning θ around $\theta = \frac{\pi}{3}$, one can turn off this term. Therefore, by considering all these observations, we come to the conclusion that in the metallic regime (or the gapless regime) the conventional skew scattering dominates the AHE in a system with a low concentration of magnetic impurities. Out of this very dilute regime, by tuning θ around $\frac{\pi}{2}$ and m around 1 and also exerting an external electric field perpendicular to the in-plane component of the magnetization, the AHE gets its maximal reachable value. If the extrinsic and intrinsic terms both contribute to the AHE with comparable sizes (the intermediate regime), one can observe a sign change in the anomalous Hall conductivity not only via tuning the Fermi level or the spatial orientation of the surface magnetization, but surprisingly also via tuning the concentration of the impurities, for a certain range of the other parameters. Let us highlight that the nonmonotonic behavior of the found AHE, which perfectly distinguishes it from the longitudinal conductivity, manifest itself in the found sign change. Besides, this sign change of the AHE does not occur in the absence of the magnetic impurities.

ACKNOWLEDGMENTS

The authors greatly acknowledge fruitful conversations with S. Abedinpour, W. Magnus, J. Abouie, and B. Sorée.

APPENDIX A: LONGITUDINAL MAGNETIC MEAN FREE PATHS $\lambda_i^{m,s}$

To calculate the current density of the system $\mathbf{J} = -e \sum_{\mathbf{k}} \mathbf{v}_{\mathbf{k}} f_{\mathbf{k}}$, we need to find the following three terms in the velocity of the electrons $\mathbf{v}_{\mathbf{k}} = \mathbf{v}_{0\mathbf{k}} + \mathbf{v}_{\mathbf{k}}^{\text{an}} + \mathbf{v}_{\mathbf{k}}^{\text{sj}}$ and also the following five terms in the distribution function of the Dirac fermions $f_{\mathbf{k}} = f^0 + g_{\mathbf{k}}^s + g_{\mathbf{k}}^{a1} + g_{\mathbf{k}}^{a2} + g_{\mathbf{k}}^{ad}$. These terms in the velocity of the electrons are calculated in the main text of this work. The next step is to calculate the equilibrium distribution function of the Dirac fermions. As the dynamics of these fermions during scattering off nonmagnetic impurities is isotropic, it can be treated by the widely used relaxation time scheme and therefore we do not include the nonmagnetic case in the following discussion. Here we go through the details of the calculation of all introduced corrections in the conductivity of the system that arise from scattering by magnetic impurities. Based on Eq. (25), in order to find $g_{\mathbf{k}}^p$, first the associated mean free paths λ_i^p have to be calculated. In this section, we first clarify the procedure to obtain $\lambda_i^{m,s}$. In Appendix B, Appendix C and finally in Appendix D, we go through the calculation of $\lambda_i^{m,ad}$, $\lambda_i^{m,sk1}$, and $\lambda_i^{m,sk2}$, respectively.

To find the longitudinal conductivity of the system, we need to find the distribution function of the electrons during their conventional scattering off magnetic impurities.

According to Eqs. (25) and (26), we arrive at

$$\mathbf{v}_{0\mathbf{k}} \cdot \hat{x}_i = \sum_{\mathbf{k}'} w_{\mathbf{k}\mathbf{k}'}^{(2,m)} [\lambda_i^{m,s}(\mathbf{k}) - \lambda_i^{m,s}(\mathbf{k}')], \quad (\text{A1})$$

where $w_{\mathbf{k}\mathbf{k}'}^{(2,m)}$ is transition rate of magnetic scatterings. Replacing the mean free path with its Fourier expansion $\lambda_i^{m,s}(\mathbf{k}, \theta) = \sum_{n=1}^{\infty} [\lambda_i^0(k) + \lambda_i^{m,s,c}(\mathbf{k}) \cos n\phi_{\mathbf{k}} + \lambda_i^{m,s,s}(\mathbf{k}) \sin n\phi_{\mathbf{k}}]$ leads to

$$\mathbf{v}_{0\mathbf{k}} \cdot \hat{x}_i = \sum_{\mathbf{k}'} \sum_{n=1}^{\infty} w_{\mathbf{k}\mathbf{k}'}^{(2,m)} (\lambda_{i,n}^{m,s,c} [\cos n\phi_{\mathbf{k}} - \cos n\phi_{\mathbf{k}'}] + \lambda_{i,n}^{m,s,s} [\sin n\phi_{\mathbf{k}} - \sin n\phi_{\mathbf{k}'}]), \quad (\text{A2})$$

where $\hat{x}_1 = \hat{x}$ and $\hat{x}_2 = \hat{y}$. Before continuing our discussion, note that conservation of the number of particles imposes

$$N = \sum_{\mathbf{k}} f_{\mathbf{k}}^0 = \sum_{\mathbf{k}} (f_{\mathbf{k}}^0 + g_{\mathbf{k}}^s + g_{\mathbf{k}}^{ad} + g_{\mathbf{k}}^{a1} + g_{\mathbf{k}}^{a2}). \quad (\text{A3})$$

Therefore $\sum_{\mathbf{k}} (g_{\mathbf{k}}^s + g_{\mathbf{k}}^{ad} + g_{\mathbf{k}}^{a1} + g_{\mathbf{k}}^{a2}) = 0$, and hence all the constant terms in the Fourier expansions are zero. After some calculations, we obtain

$$\lambda_i^{m,s}(\mathbf{k}, \theta) = \frac{\alpha_i^{m,s,0} + (\alpha_i^{m,s,c} + \delta_{i,1}) \cos \phi_{\mathbf{k}} + (\alpha_i^{m,s,s} + \delta_{i,2}) \sin \phi_{\mathbf{k}}}{2(\beta_{\mathbf{k}} \cos \phi_{\mathbf{k}} + 1)(\gamma_{\mathbf{k}}^2 \cos 2\theta + 1)} \lambda_0^{m,s}, \quad (\text{A4})$$

where $\beta_{\mathbf{k}} = \frac{\gamma_{\mathbf{k}} \sqrt{1-\gamma_{\mathbf{k}}^2} \sin 2\theta}{\gamma_{\mathbf{k}}^2 \cos 2\theta + 1}$, $\alpha_i^{m,s,0} = \gamma_{\mathbf{k}} \sqrt{1-\gamma_{\mathbf{k}}^2} \sin 2\theta \frac{\lambda_{i,1}^{m,s,c}}{\lambda_0^{m,s}}$, $\alpha_i^{m,s,c} = (1-\gamma_{\mathbf{k}}^2)(2 \sin^2 \theta - 1) \frac{\lambda_{i,1}^{m,s,c}}{\lambda_0^{m,s}}$, $\alpha_i^{m,s,s} = (\gamma_{\mathbf{k}}^2 - 1) \frac{\lambda_{i,1}^{m,s,s}}{\lambda_0^{m,s}}$ and $\lambda_0^{m,s} = \frac{4\hbar^3 v_F^3 \sqrt{1-\gamma_{\mathbf{k}}^2}}{n_{\text{im}} J^2 S_m^2 \varepsilon_{\mathbf{k}}}$. As it is clear from the equations above, $\lambda_{i,1}^{m,s,c}$ and $\lambda_{i,1}^{m,s,s}$ are the only two required Fourier coefficients of $\lambda_i^{m,s}$, as the other higher-order Fourier coefficients ($n > 1$) are a function of these two primary coefficients. These crucial Fourier coefficients can be obtained straightforwardly as follows:

$$\begin{aligned} \pi \lambda_{i,1}^{m,s,c} - \int_0^{2\pi} \frac{\alpha_i^{m,s,0} + (\alpha_i^{m,s,c} + \delta_{i,1}) \cos \phi_{\mathbf{k}} + (\alpha_i^{m,s,s} + \delta_{i,2}) \sin \phi_{\mathbf{k}}}{2(\beta_{\mathbf{k}} \cos \phi_{\mathbf{k}} + 1)(\gamma_{\mathbf{k}}^2 \cos 2\theta + 1)} \lambda_0^{m,s} \cos \phi_{\mathbf{k}} d\phi_{\mathbf{k}} &= 0, \\ \pi \lambda_{i,1}^{m,s,s} - \int_0^{2\pi} \frac{\alpha_i^{m,s,0} + (\alpha_i^{m,s,c} + \delta_{i,1}) \cos \phi_{\mathbf{k}} + (\alpha_i^{m,s,s} + \delta_{i,2}) \sin \phi_{\mathbf{k}}}{2(\beta_{\mathbf{k}} \cos \phi_{\mathbf{k}} + 1)(\gamma_{\mathbf{k}}^2 \cos 2\theta + 1)} \lambda_0^{m,s} \sin \phi_{\mathbf{k}} d\phi_{\mathbf{k}} &= 0. \end{aligned} \quad (\text{A5})$$

After solving the above set of integral equations, we arrive at

$$\lambda_{1,1}^{m,s,c} = \frac{4 \hbar^3 v_F^3}{n_{\text{im}} J^2 S_m^2 \varepsilon_{\mathbf{k}}} \frac{\sqrt{1-\gamma_{\mathbf{k}}^2}}{1 + \Gamma_{\mathbf{k}} + (1 + \Gamma_{\mathbf{k}} \gamma_{\mathbf{k}}^2) \cos 2\theta}, \quad \lambda_{1,1}^{m,s,s} = 0, \quad (\text{A6})$$

$$\lambda_{2,1}^{m,s,c} = 0, \quad \lambda_{2,1}^{m,s,s} = \frac{4 \hbar^3 v_F^3}{n_{\text{im}} J^2 S_m^2 \varepsilon_{\mathbf{k}}} \frac{\sqrt{1-\gamma_{\mathbf{k}}^2}}{1 - \gamma_{\mathbf{k}}^2 + (1 + \Gamma_{\mathbf{k}})(1 + \gamma_{\mathbf{k}}^2 \cos 2\theta)}, \quad (\text{A7})$$

where $\Gamma = (1 - \frac{\gamma_{\mathbf{k}}^2(1-\gamma_{\mathbf{k}}^2) \sin^2 2\theta}{(1+\gamma_{\mathbf{k}}^2 \cos 2\theta)^2})^{1/2}$. Putting the found nonzero Fourier coefficient $\lambda_{1,1}^{m,s,c}$ and $\lambda_{2,1}^{m,s,s}$ in Eq. (A4) gives

$$\lambda_1^{m,s} = \frac{A_{\mathbf{k}} \cos \phi_{\mathbf{k}} + \gamma_{\mathbf{k}} \sin 2\theta \sqrt{1-\gamma_{\mathbf{k}}^2}}{[1 + \beta_{\mathbf{k}} \cos \phi_{\mathbf{k}}][1 + \gamma_{\mathbf{k}}^2 \cos 2\theta][A + [1 - \gamma_{\mathbf{k}}^2] \cos 2\theta]} \frac{\lambda_0^{m,s}}{2}, \quad (\text{A8})$$

$$\lambda_2^{m,s} = \frac{(1 + \Gamma_{\mathbf{k}}) \sin \phi_{\mathbf{k}}}{[1 + \beta_{\mathbf{k}} \cos \phi_{\mathbf{k}}][1 + A_{\mathbf{k}} - \gamma_{\mathbf{k}}^2]} \frac{\lambda_0^{m,s}}{2}, \quad (\text{A9})$$

where $A_{\mathbf{k}} = (1 + \Gamma_{\mathbf{k}})(1 + \gamma_{\mathbf{k}}^2 \cos 2\theta)$. Therefore the resultant correction to the distribution function of the electrons due to the conventional scattering of electrons from magnetic impurities is

$$g_{\mathbf{k}}^{m,s} = eE \left[\frac{A_{\mathbf{k}} \cos \phi_{\mathbf{k}} + \gamma_{\mathbf{k}} \sin 2\theta \sqrt{1-\gamma_{\mathbf{k}}^2}}{[1 + \beta_{\mathbf{k}} \cos \phi_{\mathbf{k}}][1 + \gamma_{\mathbf{k}}^2 \cos 2\theta][A_{\mathbf{k}} + [1 - \gamma_{\mathbf{k}}^2] \cos 2\theta]} \frac{\lambda_0^{m,s}}{2} \cos \chi + \frac{(1 + \Gamma_{\mathbf{k}}) \sin \phi_{\mathbf{k}}}{[1 + \beta_{\mathbf{k}} \cos \phi_{\mathbf{k}}][1 + A_{\mathbf{k}} - \gamma_{\mathbf{k}}^2]} \frac{\lambda_0^{m,s}}{2} \sin \chi \right] \partial_{\varepsilon_{\mathbf{k}}} f^0. \quad (\text{A10})$$

APPENDIX B: SIDE-JUMP-ASSOCIATED MEAN FREE PATHS $\lambda_i^{m,ad}$

As it was indicated in the main text, electrons during scattering off magnetic impurities undergo a side jump which changes the velocity of the electrons and also their distribution function. This leads to the following two corrections to the conductivity:

$\sigma_{ij}^{m.sj}$ and $\sigma_{ij}^{m.ad}$. Since we have already found the associated distribution function $g_{\mathbf{k}}^{m.s}$, we needn't to calculate $\sigma_{ij}^{m.sj}$, thus in this section, we just present the details of calculating $\sigma_{ij}^{m.ad}$. As before, we ignore the side jump of the electrons during their skew scattering. As we did to calculate $g_{\mathbf{k}}^{m.ad}$, we replace $\lambda_i^{m.ad}$ in Eq. (27) with their Fourier expansions $\lambda_i^{m.ad}(\mathbf{k}, \theta) = \sum_{n=1}^{\infty} [\lambda_{i,n}^{m.ad,c} \cos n\phi_{\mathbf{k}} + \lambda_{i,n}^{m.ad,s} \sin n\phi_{\mathbf{k}}]$. By assuming that the external electric field is exerted along \hat{x}_i , Eq. (27) is converted into

$$\mathbf{v}_{\mathbf{k}}^{m.sj} \cdot \hat{x}_i = \sum_{\mathbf{k}'} \sum_{n=1}^{\infty} w_{\mathbf{k}\mathbf{k}'}^{(2,m)} (\lambda_{i,n}^{m.ad,c} [\cos n\phi_{\mathbf{k}} - \cos n\phi_{\mathbf{k}'}] + \lambda_{i,n}^{m.ad,s} [\sin n\phi_{\mathbf{k}} - \sin n\phi_{\mathbf{k}'}]). \quad (\text{B1})$$

Using the already found functions $\mathbf{v}_{\mathbf{k}}^{m.sj}$ in Eq. (35), we arrive at

$$\lambda_i^{m.ad}(\mathbf{k}, \theta) = \frac{\alpha_i^{m.ad,0} + [\alpha_i^{m.ad,c} - \delta_{i,2}] \cos \phi_{\mathbf{k}} + (\alpha_i^{m.ad,s} + [2 - \cos 2\theta] \delta_{i,1}) \sin \phi_{\mathbf{k}}}{2[\beta_{\mathbf{k}} \cos \phi_{\mathbf{k}} + 1][\gamma_{\mathbf{k}}^2 \cos 2\theta + 1]} \lambda_0^{m.ad}, \quad (\text{B2})$$

where $\alpha_i^{m.ad,0} = \gamma_{\mathbf{k}} \sqrt{1 - \gamma_{\mathbf{k}}^2} \sin 2\theta \frac{\lambda_{i,1}^{m.ad,c}}{\lambda_0^{m.ad}}$, $\alpha_i^{m.ad,c} = (1 - \gamma_{\mathbf{k}}^2)(2 \sin^2 \theta - 1) \frac{\lambda_{i,1}^{m.ad,c}}{\lambda_0^{m.ad}}$, $\alpha_i^{m.ad,s} = (\gamma_{\mathbf{k}}^2 - 1) \frac{\lambda_{i,1}^{m.ad,s}}{\lambda_0^{m.ad}}$, and $\lambda_0^{m.ad} = \frac{\hbar v_F}{2\varepsilon_{\mathbf{k}}} \gamma_{\mathbf{k}} \sqrt{1 - \gamma_{\mathbf{k}}^2}$. Finally we have to solve the set of equations

$$\begin{aligned} \pi \lambda_{i,1}^{m.ad,c} - \int_0^{2\pi} \frac{\alpha_i^{m.ad,0} + [\alpha_i^{m.ad,c} - \delta_{i,2}] \cos \phi_{\mathbf{k}} + (\alpha_i^{m.ad,s} + [2 - \cos 2\theta] \delta_{i,1}) \sin \phi_{\mathbf{k}}}{2[\beta_{\mathbf{k}} \cos \phi_{\mathbf{k}} + 1][\gamma_{\mathbf{k}}^2 \cos 2\theta + 1]} \lambda_0^{m.ad} \cos \phi_{\mathbf{k}} d\phi_{\mathbf{k}} &= 0 \\ \pi \lambda_{i,1}^{m.ad,s} - \int_0^{2\pi} \frac{\alpha_i^{m.ad,0} + [\alpha_i^{m.ad,c} - \delta_{i,2}] \cos \phi_{\mathbf{k}} + (\alpha_i^{m.ad,s} + [2 - \cos 2\theta] \delta_{i,1}) \sin \phi_{\mathbf{k}}}{2[\beta_{\mathbf{k}} \cos \phi_{\mathbf{k}} + 1][\gamma_{\mathbf{k}}^2 \cos 2\theta + 1]} \lambda_0^{m.ad} \sin \phi_{\mathbf{k}} d\phi_{\mathbf{k}} &= 0. \end{aligned} \quad (\text{B3})$$

Their solution is

$$\lambda_{1,1}^{m.ad,s} = \frac{[\sqrt{1 - \beta_{\mathbf{k}}^2} - 1][\cos 2\theta - 2]}{\beta_{\mathbf{k}}^2 [1 + \gamma_{\mathbf{k}}^2 \cos 2\theta] + [\sqrt{1 - \beta_{\mathbf{k}}^2} - 1][\gamma_{\mathbf{k}}^2 - 1]} \lambda_0^{m.ad}, \quad \lambda_{1,1}^{m.ad,c} = 0, \quad (\text{B4})$$

$$\lambda_{2,1}^{m.ad,c} = -\frac{1}{[[\sqrt{1 - \beta_{\mathbf{k}}^2} - \beta_{\mathbf{k}}^2] \gamma_{\mathbf{k}}^2 + 1] \cos 2\theta - \beta_{\mathbf{k}}^2 + \sqrt{1 - \beta_{\mathbf{k}}^2} + \beta_{\mathbf{k}} \gamma_{\mathbf{k}} \sqrt{1 - \gamma_{\mathbf{k}}^2} \sin 2\theta + 1} \lambda_0^{m.ad}, \quad \lambda_{2,1}^{m.ad,s} = 0. \quad (\text{B5})$$

Inserting $\lambda_{1,1}^{m.ad,s}$ and $\lambda_{2,1}^{m.ad,c}$ in Eq. (B2) leads to

$$\lambda_1^{m.ad}(\mathbf{k}, \theta) = \frac{(2 - \cos 2\theta) \sin \phi_{\mathbf{k}}}{(1 + \gamma_{\mathbf{k}}^2 \cos 2\theta + \beta_{\mathbf{k}}^{-1} [\sqrt{1 - \beta_{\mathbf{k}}^2} - 1][\gamma_{\mathbf{k}}^2 - 1]) [1 + \beta_{\mathbf{k}} \cos \phi_{\mathbf{k}}]} \lambda_0^{m.ad}, \quad (\text{B6})$$

$$\lambda_2^{m.ad}(\mathbf{k}, \theta) = -\frac{\gamma_{\mathbf{k}} \sqrt{1 - \gamma_{\mathbf{k}}^2} \sin 2\theta + c_{\mathbf{k}} \cos \phi_{\mathbf{k}}}{2[1 + \beta_{\mathbf{k}} \cos \phi_{\mathbf{k}}][1 + \gamma_{\mathbf{k}}^2 \cos 2\theta][c_{\mathbf{k}} + (1 - \gamma_{\mathbf{k}}^2) \cos 2\theta]} \lambda_0^{m.ad}, \quad (\text{B7})$$

where $c_{\mathbf{k}} = (1 - \beta_{\mathbf{k}}^2 + \sqrt{1 - \beta_{\mathbf{k}}^2})(1 + \gamma_{\mathbf{k}}^2 \cos 2\theta) + \beta_{\mathbf{k}} \gamma_{\mathbf{k}} \sqrt{1 - \gamma_{\mathbf{k}}^2} \sin 2\theta$.

Finally, the associated correction to the distribution function of the electrons arising from the side jump can be written as, based on Eq. (25),

$$g_{\mathbf{k}}^{m.ad} = \frac{eE\lambda_0^{m.ad}\partial_{\varepsilon_{\mathbf{k}}}f^0}{[1 + \beta_{\mathbf{k}} \cos \phi_{\mathbf{k}}]} \left[\frac{(2 - \cos 2\theta) \sin \phi_{\mathbf{k}} \cos \chi}{(1 + \gamma_{\mathbf{k}}^2 \cos 2\theta + \beta_{\mathbf{k}}^{-1} [\sqrt{1 - \beta_{\mathbf{k}}^2} - 1][\gamma_{\mathbf{k}}^2 - 1])} - \frac{\gamma_{\mathbf{k}} \sqrt{1 - \gamma_{\mathbf{k}}^2} \sin 2\theta + c_{\mathbf{k}} \cos \phi_{\mathbf{k}}}{2[1 + \gamma_{\mathbf{k}}^2 \cos 2\theta][c_{\mathbf{k}} + (1 - \gamma_{\mathbf{k}}^2) \cos 2\theta]} \sin \chi \right]. \quad (\text{B8})$$

APPENDIX C: CONVENTIONAL SKEW SCATTERING ASSOCIATED MEAN FREE PATH $\lambda_i^{m.sk1}$

The conventional and intrinsic skew scattering contribute to the conductivity of the system via changing the distribution function of the electrons, as the velocity of the electrons does not change, in contrary to the side-jump effect. Based on Eq. (21),

$$g_{\mathbf{k}}^{m.a1} = \frac{\sum_{\mathbf{k}'} w_{\mathbf{k}\mathbf{k}'}^{(2,m)} g_{\mathbf{k}'}^{m.a1} + \sum_{\mathbf{k}'} w_{\mathbf{k}\mathbf{k}'}^{(3a,m)} (g_{\mathbf{k}'}^{m.s} - g_{\mathbf{k}}^{m.s})}{\sum_{\mathbf{k}'} w_{\mathbf{k}\mathbf{k}'}^{(2,m)}}. \quad (\text{C1})$$

Since $g_k^{m,s}$ has been already found, we just need to find $g_k^{m,a1}$. By using Eq. (50), it can be straightforwardly proven that $\sum_{k'} w_{kk'}^{(3a,m)} = 0$. Therefore Eq. (C2) can be rewritten in terms of the mean free paths as

$$\lambda_i^{m,a1}(\mathbf{k}, \theta) = \frac{\sum_{k'} w_{kk'}^{(3a,m)} \lambda_i^{m,s}(\mathbf{k}', \theta) + \sum_{k'} w_{kk'}^{(2,m)} \lambda_i^{m,a1}(\mathbf{k}', \theta)}{\sum_{k'} w_{kk'}^{(2,m)}}. \quad (\text{C2})$$

Using the Fourier expansions of these mean free paths $\lambda_i^{m,a1}(\mathbf{k}, \theta) = \sum_{n=1}^{\infty} [\lambda_i^{m,a1,c}(k) \cos n\phi_k + \lambda_i^{m,a1,s}(k) \sin n\phi_k]$ leads to

$$\lambda_i^{m,a1}(\mathbf{k}, \theta) = \frac{\alpha_i^{m,a1,0} + [\alpha_i^{m,a1,c} - \delta_{i,2} \frac{JS_m \cos \theta k^2}{2\epsilon_k} \lambda_{i,1}^{m,s,s}] \cos \phi_k + [\alpha_i^{m,a1,s} + \delta_{i,1} \frac{JS_m \cos \theta k^2}{2\epsilon_k} \lambda_{i,1}^{m,s,c}] \sin \phi_k}{2(1 + \gamma_k^2 \cos 2\theta)(1 + \beta_k \cos \phi_k)}, \quad (\text{C3})$$

where $\alpha_i^{m,a1,0} = \gamma_k \sqrt{1 - \gamma_k^2} \sin 2\theta \lambda_{i,1}^{m,a1,c}$, $\alpha_i^{m,a1,c} = (1 - \gamma_k^2)(2 \sin^2 \theta - 1) \lambda_{i,1}^{m,a1,c}$, $\alpha_i^{m,a1,s} = (\gamma_k^2 - 1) \lambda_{i,1}^{m,a1,s}$. Four unknown crucial Fourier coefficients $\lambda_{i,1}^{m,a1,c}$ and $\lambda_{i,1}^{m,a1,s}$ can be found through solving a set of equations such Eqs. (A5) and (B3). After solving this set of equations, we arrive at

$$\lambda_{1,1}^{m,a1,s} = \frac{\hbar v_F}{J n_{\text{im}} S_m} \frac{2(1 - \gamma_k^2) \sqrt{1 - \gamma_k^2} \cos \theta}{[1 + \Gamma_k + \cos 2\theta + \gamma_k^2 \Gamma_k \cos 2\theta][2 + \Gamma_k + \gamma_k^2 \Gamma_k \cos 2\theta - 2\gamma_k^2 \sin^2 \theta]}, \quad (\text{C4})$$

$$\lambda_{2,1}^{m,a1,c} = \frac{\hbar v_F}{J n_{\text{im}} S_m} \frac{4(1 - \Gamma_k) \sqrt{1 - \gamma_k^2} (1 + \gamma_k^2 \cos 2\theta) \cos \theta}{[\gamma_k^2 (\Gamma_k + 1) \cos 2\theta - \gamma_k^2 + \Gamma_k + 2][\gamma_k^2 (\Gamma_k \cos 4\theta + \Gamma_k - 2) + 2(\Gamma_k - 1) \cos 2\theta]}, \quad (\text{C5})$$

and $\lambda_{1,1}^{m,a1,c} = \lambda_{2,1}^{m,a1,s} = 0$. Inserting the resultant nonzero Fourier coefficients in Eq. (C3), one obtains the mean free paths of the electrons during magnetic conventional skew scattering:

$$\lambda_1^{m,a1}(\mathbf{k}, \theta) = -\frac{\hbar v_F}{J S_m n_{\text{im}}} \frac{(1 + \Gamma_k) \cos \theta \sin \phi_k}{[(\Gamma_k \gamma_k^2 + 1) \cos 2\theta + \Gamma_k + 1][p_k + p_k \beta_k \cos \phi_k]}, \quad (\text{C6})$$

$$\lambda_2^{m,a1}(\mathbf{k}, \theta) = \frac{\hbar v_F}{J S_m n_{\text{im}}} \frac{\cos \theta \{[(4 - 4\Gamma_k) \cos 2\theta + (2\Gamma_k - 3)\gamma_k^2 + (2\Gamma_k - 1)\gamma_k^2 \cos 4\theta] \cos \phi_k + B_k\}}{[1 + \gamma_k^2 \cos 2\theta][\Gamma_k \gamma_k^2 \cos 4\theta + (2\Gamma_k - 2) \cos 2\theta + (\Gamma_k - 2)\gamma_k^2][p_k + p_k \beta_k \cos \phi_k]}, \quad (\text{C7})$$

$p_k = \{\gamma^2[(\Gamma_k + 1) \cos 2\theta - 1] + \Gamma_k + 2\}(1 - \gamma_k^2)^{-3/2}$, $B_k = 2(1 - \gamma_k^2)^{-1/2} \gamma_k (\Gamma_k - 1)(1 + \gamma_k^2 \cos 2\theta) \sin 2\theta$.

Finally, the associated correction to the distribution function of the electrons arising from the side jump can be written, based on Eq. (25), as

$$g_k^{m,a1} = \alpha^{m,a1} \left(\frac{[(4 - 4\Gamma_k) \cos 2\theta - 2\gamma_k^2 + (2\Gamma_k - 1)\gamma_k^2 (\cos 4\theta + 1)] \cos \phi_k + B_k}{(1 + \gamma_k^2 \cos 2\theta) (\Gamma_k \gamma_k^2 \cos 4\theta + (2\Gamma_k - 2) \cos 2\theta + (\Gamma_k - 2)\gamma_k^2)} \sin \chi - \frac{(1 + \Gamma_k) \sin \phi_k \cos \chi}{(\Gamma_k \gamma_k^2 + 1) \cos 2\theta + \Gamma_k + 1} \right), \quad (\text{C8})$$

with $\alpha^{m,a1} = \frac{eE \partial_{\epsilon_k} f^0}{p_k + p_k \beta_k \cos \phi_k} \frac{\hbar v_F}{J S_m n_{\text{im}}}$.

APPENDIX D: INTRINSIC SKEW SCATTERING ASSOCIATED MEAN FREE PATH $\lambda_i^{m,a2}$

Like the conventional skew scattering, this contribution to the skew scattering just alters the distribution function of the electrons and leaves the velocity of the electrons unchanged. Using Eq. (23), which connects the conventional magnetic scattering of electrons to their intrinsic magnetic skew scattering, we arrive at

$$\sum_{k'} w_{kk'}^{(4m)} [\lambda_i^{m,s}(\mathbf{k}) - \lambda_i^{m,s}(\mathbf{k}')] + \sum_{k'} w_{kk'}^{(2,m)} [\lambda_i^{m,a2}(\mathbf{k}) - \lambda_i^{m,a2}(\mathbf{k}')] = 0, \quad (\text{D1})$$

which after rewriting gives

$$\lambda_i^{m,a2} = \frac{\sum_{k'} w_{kk'}^{(2,m)} \lambda_i^{m,a2}(\mathbf{k}') + w_{kk'}^{(4,m)} [\lambda_i^{m,s}(\mathbf{k}') - \lambda_i^{m,s}(\mathbf{k})]}{\sum_{k'} w_{kk'}^{(2,m)}}. \quad (\text{D2})$$

Applying the Fourier expansions of the mean free paths $\lambda_i^{m,a2}$ as $\lambda_i^{m,a2}(\mathbf{k}) = \sum_{n=1}^{\infty} [\lambda_{i,n}^{m,a2,c} \cos n\phi_k + \lambda_{i,n}^{m,a2,s} \sin n\phi_k]$ leads to

$$\lambda_i^{m,a2} = \frac{\sum_{k',n} w_{kk'}^{(2,m)} [\lambda_{i,n}^{m,a2,c} \cos n\phi_{k'} + \lambda_{i,n}^{m,a2,s} \sin n\phi_{k'}] + \sum_{k'} w_{kk'}^{(4,m)} [\lambda_i^{m,s}(\mathbf{k}') - \lambda_i^{m,s}(\mathbf{k})]}{\sum_{k'} w_{kk'}^{(2,m)}}. \quad (\text{D3})$$

Using the already found $w_{kk'}^{(2,m)}$, $w_{kk'}^{(4,m)}$ and $\lambda_i^{m,s}(\mathbf{k}')$, we arrive at

$$\begin{aligned} \lambda_i^{m,a2} = & \left([\gamma_k^3 - \gamma_k] [2 \cos 2\theta + 1] \lambda_{i,1}^{m,s,c} \sin \phi_k - \lambda_{i,1}^{m,s,s} [\cos 2\theta + 2] \cos \phi_k \right) - \gamma_k^2 \sqrt{1 - \gamma_k^2} \lambda_{i,1}^{m,s,s} \sin 2\theta \alpha_1^{m,a2} \\ & + \left(\frac{1}{2} [\gamma_k^2 - 1] \lambda_{i,1}^{m,a2,s} \sin \phi_k + \frac{1}{2} [\gamma_k^2 - 1] \lambda_{i,1}^{m,a2,c} \cos 2\theta \cos \phi_k + \frac{1}{2} \gamma_k \sqrt{1 - \gamma_k^2} \lambda_{i,1}^{m,a2,c} \sin 2\theta \right) \alpha_0^{m,a2} \\ & - 4 \lambda_i^{m,s} \gamma_k \sqrt{1 - \gamma_k^2} \sin \phi_k \sin 2\theta \alpha_1^{m,a2}, \end{aligned} \quad (D4)$$

where $\alpha_0^{m,a2} = \frac{1}{\gamma_k^2 \cos 2\theta + \gamma_k \sqrt{1 - \gamma_k^2} \sin 2\theta \cos \phi_k + 1}$, and $\alpha_1^{m,a2} = \frac{n_{\text{im}} J_m^2 S_m^2}{8 \hbar^2 v_F^2} \frac{1}{\gamma_k^2 \cos 2\theta + \gamma_k \sqrt{1 - \gamma_k^2} \sin 2\theta \cos \phi_k + 1}$. These two crucial nonzero Fourier coefficients $\lambda_{1,1}^{m,s,c}$ and $\lambda_{2,1}^{m,s,s}$ are given in Eqs. (A6) and (A7). Four unknown crucial Fourier coefficients $\lambda_{i,1}^{m,a2,c}$ and $\lambda_{i,1}^{m,a2,s}$ can be obtained by solving a set of equations as we did in Eq. (A5) or (B3). After solving this set of equations, we arrive at

$$\lambda_{1,1}^{m,a2,s} \left[\frac{\hbar v_F}{\varepsilon_k} \right] = \frac{8(\gamma_k - \Gamma_k \gamma_k) (\gamma_k^4 (\Gamma_k - 2)(\Gamma_k + 1) + \gamma_k^2 (\Gamma_k - 1)(\gamma_k^2 \Gamma_k + 1) \cos 4\theta - \xi_k \cos 2\theta + \gamma_k^2 + 2\Gamma_k^2 + \Gamma_k - 2)}{\Gamma_k \sqrt{1 - \gamma_k^2} ([\gamma_k^2 \Gamma_k + 1] \cos 2\theta + \Gamma_k + 1) ((\cos 2\theta [\Gamma_k - 1] - \sin^2 2\theta) \gamma_k^2 + \Gamma_k - 1)}, \quad (D5)$$

$$\lambda_{2,1}^{m,a2,c} \left[\frac{\hbar v_F}{\varepsilon_k} \right] = \frac{16 \gamma_k \sqrt{1 - \gamma_k^2} [\Gamma_k - 1] (-\gamma_k^2 \cos 4\theta + [2\gamma_k^2 + 1] \cos 2\theta + 2\gamma_k^2 + 2)}{(\gamma_k^2 (\Gamma_k + 1) \cos 2\theta - \gamma_k^2 + \Gamma_k + 2) (\gamma_k^2 (\Gamma_k \cos 4\theta + \Gamma_k - 2) + 2(\Gamma_k - 1) \cos 2\theta)}, \quad (D6)$$

where $\xi_k = \gamma_k^2 (\Gamma_k [\gamma_k^2 - 4\Gamma_k + 1] + 4) - 2\Gamma_k$ and $\lambda_{1,1}^{m,a2,c} = \lambda_{2,1}^{m,a2,s} = 0$. We can express the correction to the distribution function of the electrons due to the magnetic intrinsic skew scattering as

$$\begin{aligned} g_k^{m,a2} = & \left([\gamma_k^3 - \gamma_k] [2 \cos 2\theta + 1] \lambda_{1,1}^{m,s,c} \sin \phi_k - \lambda_{1,1}^{m,s,s} [\cos 2\theta + 2] \cos \phi_k \right) - \gamma_k^2 \sqrt{1 - \gamma_k^2} \lambda_{1,1}^{m,s,s} \sin 2\theta \alpha_2^{m,a2} \\ & + \left(\frac{1}{2} [\gamma_k^2 - 1] \lambda_{1,1}^{m,a2,s} \sin \phi_k + \frac{1}{2} [\gamma_k^2 - 1] \lambda_{1,1}^{m,a2,c} \cos 2\theta \cos \phi_k + \frac{1}{2} \gamma_k \sqrt{1 - \gamma_k^2} \lambda_{1,1}^{m,a2,c} \sin 2\theta \right) \alpha_3^{m,a2} \\ & - 4 \lambda_1^{m,s} \gamma_k \sqrt{1 - \gamma_k^2} \sin \phi_k \sin 2\theta \alpha_2^{m,a2} \\ & + \left([\gamma_k^3 - \gamma_k] [2 \cos 2\theta + 1] \lambda_{2,1}^{m,s,c} \sin \phi_k - \lambda_{2,1}^{m,s,s} [\cos 2\theta + 2] \cos \phi_k \right) - \gamma_k^2 \sqrt{1 - \gamma_k^2} \lambda_{2,1}^{m,s,s} \sin 2\theta \alpha_4^{m,a2} \\ & + \left(\frac{1}{2} [\gamma_k^2 - 1] \lambda_{2,1}^{m,a2,s} \sin \phi_k + \frac{1}{2} [\gamma_k^2 - 1] \lambda_{2,1}^{m,a2,c} \cos 2\theta \cos \phi_k + \frac{1}{2} \gamma_k \sqrt{1 - \gamma_k^2} \lambda_{2,1}^{m,a2,c} \sin 2\theta \right) \alpha_5^{m,a2} \\ & - 4 \lambda_2^{m,s} \gamma_k \sqrt{1 - \gamma_k^2} \sin \phi_k \sin 2\theta \alpha_4^{m,a2}, \end{aligned} \quad (D7)$$

$$\alpha_2^{m,a2} = eE \partial_{\varepsilon_k} f^0 \alpha_1^{m,a2} \cos \chi, \alpha_3^{m,a2} = eE \partial_{\varepsilon_k} f^0 \alpha_0^{m,a2} \cos \chi, \alpha_4^{m,a2} = eE \partial_{\varepsilon_k} f^0 \alpha_1^{m,a2} \sin \chi, \alpha_5^{m,a2} = eE \partial_{\varepsilon_k} f^0 \alpha_0^{m,a2} \sin \chi.$$

As we already proved $\lambda_{1,1}^{m,s,s} = 0$ and $\lambda_{2,1}^{m,s,c} = 0$, finally we can write the final expression for the correction to the distribution function of the electrons as

$$\begin{aligned} g_k^{m,a2} = & \sin \phi_k \left([\gamma_k^3 - \gamma_k] [2 \cos 2\theta + 1] \lambda_{1,1}^{m,s,c} \alpha_2^{m,a2} + \frac{1}{2} [\gamma_k^2 - 1] \lambda_{1,1}^{m,a2,s} \alpha_3^{m,a2} - 4 \lambda_1^{m,s} \gamma_k \sqrt{1 - \gamma_k^2} \sin 2\theta \alpha_2^{m,a2} \right) \\ & + \frac{1}{2} [\gamma_k^2 - 1] \lambda_{1,1}^{m,a2,c} \cos 2\theta \alpha_3^{m,a2} \cos \phi_k + \frac{1}{2} \gamma_k \sqrt{1 - \gamma_k^2} \lambda_{1,1}^{m,a2,c} \sin 2\theta \alpha_3^{m,a2} \\ & + \sin \phi_k \left([\gamma_k^3 - \gamma_k] [2 \cos 2\theta + 1] \lambda_{2,1}^{m,s,c} \alpha_4^{m,a2} + \frac{1}{2} [\gamma_k^2 - 1] \lambda_{2,1}^{m,a2,s} \alpha_5^{m,a2} - 4 \lambda_2^{m,s} \gamma_k \sqrt{1 - \gamma_k^2} \sin 2\theta \alpha_4^{m,a2} \right) \\ & + \left(\lambda_{2,1}^{m,s,s} [\cos 2\theta + 2] [\gamma_k - \gamma_k^3] \alpha_4^{m,a2} + \frac{1}{2} \alpha_5^{m,a2} [\gamma_k^2 - 1] \lambda_{2,1}^{m,a2,c} \cos 2\theta \right) \cos \phi_k \\ & - \frac{1}{2} \gamma_k \sqrt{1 - \gamma_k^2} \sin 2\theta (2\alpha_4^{m,a2} \gamma_k \lambda_{2,1}^{m,s,s} - \lambda_{2,1}^{m,a2,c} \alpha_5^{m,a2}). \end{aligned} \quad (D8)$$

[1] L. Fu, C. L. Kane, and E. J. Mele, *Phys. Rev. Lett.* **98**, 106803 (2007).
 [2] X. L. Qi and S. C. Zhang, *Rev. Mod. Phys.* **83**, 1057 (2011).
 [3] B. A. Bernevig, T. L. Hughes, and S. C. Zhang, *Science* **314**, 1757 (2006).
 [4] M. Z. Hasan and C. L. Kane, *Rev. Mod. Phys.* **82**, 3045 (2010).
 [5] L. Fu, *Phys. Rev. Lett.* **106**, 106802 (2011).

[6] S. Q. Shen, *Topological Insulators: Dirac Equation in Condensed Matters* (Springer-Verlag, Berlin, 2012).
 [7] P. Roushan, J. Seo, C. V. Parker, Y. S. Hor, D. Hsieh, D. Qian, A. Richardella, M. Z. Hasan, R. J. Cava, and A. Yazdani, *Nature (London)* **460**, 1106 (2009).
 [8] M. Liu, J. Zhang, C. Z. Chang, Z. Zhang, X. Feng, K. Li, K. He, L. L. Wang, X. Chen, X. Dai, Z. Fang, Q. K. Xue, X. Ma, and Y. Wang, *Phys. Rev. Lett.* **108**, 036805 (2012).

- [9] J. E. Moore and L. Balents, *Phys. Rev. B* **75**, 121306(R) (2007).
- [10] X. L. Qi, T. L. Hughes, and S. C. Zhang, *Phys. Rev. B* **78**, 195424 (2008).
- [11] D. Hsieh, Y. Xia, D. Qian, L. Wray, F. Meier, J. H. Dil, J. Osterwalder, L. Patthey, A. V. Fedorov, H. Lin *et al.*, *Phys. Rev. Lett.* **103**, 146401 (2009).
- [12] D. Culcer, *Physica E* **44**, 860 (2012).
- [13] D. Culcer, E. H. Hwang, Tudor D. Stanescu, and S. Das Sarma, *Phys. Rev. B* **82**, 155457 (2010).
- [14] R. Yu, W. Zhang, H. J. Zhang, S. C. Zhang, X. Dai, and Z. Fang, *Science* **329**, 61 (2010).
- [15] C. Z. Chang, J. Zhang, X. Feng, J. Shen, Z. Zhang, M. Guo, K. Li, Y. Ou, P. Wei, L. L. Wang *et al.*, *Science* **340**, 167 (2013).
- [16] X. Kou, S. T. Guo, Y. Fan, L. Pan, M. Lang, Y. Jiang, Q. Shao, T. Nie, K. Murata, J. Tang *et al.*, *Phys. Rev. Lett.* **113**, 137201 (2014).
- [17] Y. Xing, F. Xu, K. T. Cheung, Q. F. Sun, J. Wang, and Y. Yao, *New J. Phys.* **20**, 043011 (2018).
- [18] N. Nagaosa, J. Sinova, S. Onoda, A. H. MacDonald, and N. P. Ong, *Rev. Mod. Phys.* **82**, 1539 (2010).
- [19] Y. Ni, Z. Zhang, I. C. Nlebedim, and D. C. Jiles, *IEEE Trans. Magn.* **52**, 1 (2016).
- [20] S. Das, H. Yoshikawa, and S. Nakagawa, *J. Appl. Phys.* **93**, 8098 (2003).
- [21] S. K. Wong, K. Srinivasan, R. Sbiaa, R. Law, E. Tan, and S. N. Piramanayagam, *IEEE Trans. Magn.* **46**, 2409 (2010).
- [22] W. Allen, E. G. Gwinn, T. C. Kreutz, and A. C. Gossard, *Phys. Rev. B* **70**, 125320 (2004).
- [23] T. Jungwirth, Q. Niu, and A. H. MacDonald, *Phys. Rev. Lett.* **88**, 207208 (2002).
- [24] Y. Taguchi, Y. Oohara, H. Yoshizawa, N. Nagaosa, and Y. Tokura, *Science* **291**, 2573 (2001).
- [25] H. Ishizuka and N. Nagaosa, *Sci. Adv.* **4**, eaap9962 (2018).
- [26] Z. Fang, N. Nagaosa, K. S. Takahashi, A. Asamitsu, R. Mathieu, T. Ogasawara, H. Yamada, M. Kawasaki, Y. Tokura, and K. Terakura, *Science* **302**, 92 (2003).
- [27] N. A. Sinitsyn, *J. Phys.: Condens. Matter* **20**, 023201 (2008).
- [28] N. A. Sinitsyn, Q. Niu, and A. H. MacDonald, *Phys. Rev. B* **73**, 075318 (2006).
- [29] N. A. Sinitsyn, Q. Niu, J. Sinova, and K. Nomura, *Phys. Rev. B* **72**, 045346 (2005).
- [30] K. Vyborný, A. A. Kovalev, J. Sinova, and T. Jungwirth, *Phys. Rev. B* **79**, 045427 (2009).
- [31] N. Liu, J. Teng, and Y. Li, *Nat. Commun.* **9**, 1282 (2018).
- [32] V. Keskin, B. Aktaş, J. Schmalhorst, G. Reiss, H. Zhang, J. Weischenberg, and Y. Mokrousov, *Appl. Phys. Lett.* **102**, 022416 (2013).
- [33] T. Liang, J. Lin, Q. Gibson, S. Kushwaha, M. Liu, W. Wang, H. Xiong, J. A. Sobota, M. Hashimoto, P. S. Kirchmann, Z. X. Shen, R. J. Cava, N. P. Ong *et al.*, *Nat. Phys.* **14**, 451 (2018).
- [34] N. A. Sinitsyn, A. H. MacDonald, T. Jungwirth, V. K. Dugaev, and J. Sinova, *Phys. Rev. B* **75**, 045315 (2007).
- [35] I. A. Ado1, I. A. Dmitriev, P. M. Ostrovsky, and M. Titov, *Europhys. Lett.* **111**, 37004 (2015).
- [36] I. A. Ado, I. A. Dmitriev, P. M. Ostrovsky, and M. Titov, *Phys. Rev. B* **96**, 235148 (2017).
- [37] D. Culcer and S. Das Sarma, *Phys. Rev. B* **83**, 245441 (2011).
- [38] W. Kohn and J. M. Luttinger, *Phys. Rev.* **108**, 590 (1957).
- [39] R. Karplus and J. M. Luttinger, *Phys. Rev.* **95**, 1154 (1954).
- [40] J. M. Luttinger, *Phys. Rev.* **112**, 739 (1958).
- [41] J. Smit, *Physica* **21**, 877 (1955).
- [42] J. Smit, *Physica* **24**, 39 (1958).
- [43] L. Berger, *Phys. Rev. B* **2**, 4559 (1970).
- [44] W. J. Xu, B. Zhang, Z. X. Liu, Z. Wang, W. Li, Z. B. Wu, R. H. Yu, and X. X. Zhang, *Europhys. Lett.* **90**, 27004 (2010).
- [45] W. J. Fan, L. Ma, and S. M. Zhou, *J. Phys. D: Appl. Phys.* **48**, 195004 (2015).
- [46] K. S. Takahashi, H. Ishizuka, T. Murata, Q. Y. Wang, Y. Tokura, N. Nagaosa, and M. Kawasaki, *Sci. Adv.* **4**, eaar7880 (2018).
- [47] A. Popescu, P. Rodriguez-Lopez, P. M. Haney, and L. M. Woods, *Phys. Rev. B* **97**, 140407(R) (2018).
- [48] A. Diaz-Fernandez, L. Chico, J. W. Gonzalez, and F. Dominguez-Adame, *Sci. Rep.* **7**, 8058 (2017).
- [49] Y. L. Chen, J. H. Chu, J. G. Analytis, Z. K. Liu, K. Igarashi, H. H. Kuo, X. L. Qi, S. K. Mo, R. G. Moore, and D. H. Lu *et al.*, *Science* **329**, 659 (2010).
- [50] C. Xiao, D. Li, and Z. Ma, *Phys. Rev. B* **95**, 035426 (2017).
- [51] G. D. Mahan, *Condensed Matter in a Nutshell* (Princeton University Press, Princeton, 2010).
- [52] A. Sabzalipour, J. Abouie, and S. H. Abedinpour, *J. Phys.: Condens. Matter* **27**, 115301 (2015).
- [53] G. Rosenberg and M. Franz, *Phys. Rev. B* **85**, 195119 (2012).